Spatial Variability in Seasonal Snowpack Trends across the Rio Grande Headwaters (1984–2017)

Graham A. Sexstone,[a] Colin A. Penn,[a] Glen E. Liston,[b] Kelly E. Gleason,[c] C. David Moeser,[d] and David W. Clow[a]

[a] *Colorado Water Science Center, U.S. Geological Survey, Denver, Colorado*
[b] *Cooperative Institute for Research in the Atmosphere, Fort Collins, Colorado*
[c] *Portland State University, Portland, Oregon*
[d] *New Mexico Water Science Center, U.S. Geological Survey, Albuquerque, New Mexico*

ABSTRACT: This study evaluated the spatial variability of trends in simulated snowpack properties across the Rio Grande headwaters of Colorado using the SnowModel snow evolution modeling system. SnowModel simulations were performed using a grid resolution of 100 m and 3-hourly time step over a 34-yr period (1984–2017). Atmospheric forcing was provided by phase 2 of the North American Land Data Assimilation System, and the simulations accounted for temporal changes in forest canopy from bark beetle and wildfire disturbances. Annual summary values of simulated snowpack properties [snow metrics; e.g., peak snow water equivalent (SWE), snowmelt rate and timing, and snow sublimation] were used to compute trends across the domain. Trends in simulated snow metrics varied depending on elevation, aspect, and land cover. Statistically significant trends did not occur evenly within the basin, and some areas were more sensitive than others. In addition, there were distinct trend differences between the different snow metrics. Upward trends in mean winter air temperature were 0.3°C decade^{-1}, and downward trends in winter precipitation were −52 mm decade^{-1}. Middle elevation zones, coincident with the greatest volumetric snow water storage, exhibited the greatest sensitivity to changes in peak SWE and snowmelt rate. Across the Rio Grande headwaters, snowmelt rates decreased by 20% decade^{-1}, peak SWE decreased by 14% decade^{-1}, and total snowmelt quantity decreased by 13% decade^{-1}. These snow trends are in general agreement with widespread snow declines that have been reported for this region. This study further quantifies these snow declines and provides trend information for additional snow variables across a greater spatial coverage at finer spatial resolution.

KEYWORDS: Climate change; Hydrology; Snow cover; Numerical analysis/modeling; Trends; Mountain meteorology

1. Introduction

Water availability in the western United States is largely dependent on seasonal mountain snow that accumulates in the fall, winter, and spring and melts in the spring and summer each year (e.g., Barnett et al. 2005; Li et al. 2017). Approximately 65% of the water supply comes from forested areas in this region, with the majority of snowmelt originating from mountain forests (Furniss et al. 2010). Consequently, understanding how mountain snow storage is changing as a result of changes in climate and vegetation is critically important for adapting future water management plans (Middelkoop et al. 2001). Long-term snow monitoring stations have generally reported recent widespread snow declines throughout the western United States (e.g., Chavarria and Gutzler 2018; Clow 2010; Fritze et al. 2011; Harpold et al. 2012; Knowles et al. 2006; Kunkel et al. 2016; McCabe and Clark 2005; Mote 2006; Mote et al. 2005, 2018; Regonda et al. 2005; Stewart 2009), that have been linked with shifts in the fraction of precipitation falling as snow versus rain (Knowles et al. 2006),

earlier snowmelt timing (Clow 2010), and changes in snowmelt rate (Musselman et al. 2017b). Additionally, the sensitivity of seasonal snowpacks to changing atmospheric conditions has been shown to vary spatially between climate types (Harpold and Brooks 2018), with fewer consistent changes in intercontinental regions (Harpold et al. 2012) compared to maritime regions (Regonda et al. 2005).

Despite these well documented snowpack changes, an important consideration is that snow monitoring stations are not always representative of snow in surrounding areas (Gleason et al. 2017; López-Moreno et al. 2011; Meromy et al. 2013; Molotch and Bales 2005, 2006), thus, the stations may also misrepresent changes in basin scale seasonal snow storage. Seasonal snowpacks exhibit considerable spatial variability that is driven by meteorological processes and their interactions with topography and land surface features such as forests (e.g., Elder et al. 1991) over a range of spatial scales (e.g., Blöschl 1999; Deems et al. 2006; Lopez-Moreno et al. 2015; Sexstone and Fassnacht 2014). For example, in alpine areas, wind redistribution of snow can create large snowdrifts that are not represented by station observations that are typically located below tree line. Furthermore, widespread changes in forest health, structure, and density associated with wildfire and insect disturbances (Potter and Conkling 2016; Westerling et al. 2006) have been shown to exert a strong and variable influence on snowpack dynamics and evolution (Biederman et al. 2014; Frank et al. 2019; Gleason et al. 2013; Harpold et al. 2014;

Corresponding author: Graham A. Sexstone, sexstone@usgs.gov

TABLE 1. Definitions of annual climate and snow metrics used in this study.

Annual climate/snow metric	Definition
Winter air temperature (T)	Mean winter temperature from 1 Oct to 31 May
Winter precipitation (P)	Cumulative winter precipitation from 1 Oct to 31 May
Snowfall	Total precipitation falling as snow from 1 Oct to 30 Sep
Peak SWE	Maximum snow water equivalent
SWE:P	Ratio of peak SWE to winter precipitation
Peak SWE timing	Water year (WY; from 1 Oct to 31 Sep) day peak SWE occurs
Snow-covered days	Number of days with snow on the ground
Total snowmelt	Surface-water input into the soil that occurs when SWE is greater than zero
Snowmelt rate	Rate that snow melts from peak SWE to snow disappearance (melt out)
SM50	WY day following peak SWE when half of snowpack has melted
Melt-out timing	WY day when melt out occurs
Sublimation	Total snow sublimation including surface, canopy, and blowing snow components
Effective sublimation	Ratio of total snow sublimation to winter P (sublimation:P)

Pugh and Small 2012; Sexstone et al. 2018). Small changes in snow water equivalent (SWE) within headwater regions can have substantial implications to total basin discharges (e.g., Rumsey et al. 2020). Therefore, future water management planning will need to rely on a more accurate accounting of the basinwide distribution and changes of snow water resources (Fassnacht et al. 2018).

Recent studies evaluating the spatial changes in snowpack properties using physically based modeling approaches, reanalysis products, and remote sensing observations have provided important insights into large scale patterns in changing snow dynamics from regional to global scales. Liston and Hiemstra (2011) evaluated changes in snow estimates using a snow evolution model run at 10-km spatial resolution across a pan-Arctic domain and highlighted a trend in peak SWE of -170 mm decade^{-1} across this region. Across the snow-dominated western United States, Zeng et al. (2018) used a gridded reanalysis snow product and showed significant decreases in snow mass on the order of 12% decade^{-1}. At the global extent, Hammond et al. (2018b) evaluated Moderate Resolution Imaging Spectroradiometer (MODIS) snow covered area (SCA) observations and found that decreases in snow persistence were greatest in seasonal snow zones of the Northern Hemisphere. However, finer-resolution spatial snow estimates, on the order of 100 m or finer, are likely needed to resolve key drivers of seasonal snow accumulation and ablation processes in complex mountainous environments (Mott et al. 2018) and thus provide adequate accounting of snow storage at the basin scale (e.g., Margulis et al. 2016). Physically based snow modeling applications run at fine spatiotemporal resolutions (e.g., Broxton et al. 2015; Sexstone et al. 2018; Vionnet et al. 2017) offer the potential for reproducing observed snow-property distributions and, therefore, may be able to provide further insight into how snow water resources are changing at the basin scale.

In this study, we used the SnowModel (Liston and Elder 2006b) snow evolution modeling system to simulate snowpack processes at 100-m spatial resolution over a 34-yr period (1984–2017) for the Rio Grande headwaters basin of Colorado, United States (hereafter Rio Grande headwaters), a region where seasonal snow serves as the primary source of water

supply for large areas downstream (Rango 2006). We used spatially distributed annual summary values of snowpack properties (i.e., snow metrics; Table 1) from the SnowModel simulations to compute trend analyses for each grid cell across the model domain using the nonparametric Mann–Kendall trend test. The primary objective of this research was to evaluate the finescale spatial variability of trends in simulated snowpack properties across the Rio Grande headwaters to provide further insight on how snow water resources are changing at the basin scale over time relative to long-term climate trends and episodic disturbance events.

2. Methods

a. Study area

The study area was a 140 km $\times$ 80 km model domain in the San Juan Mountains of southwestern Colorado, United States, encompassing the Rio Grande headwaters (hydrologic unit code 13010001; 3575 km^2; Fig. 1). Elevations within the modeling domain ranged from 1990 to 4293 m (North American Vertical Datum of 1988). Observations at Snowpack Telemetry (SNOTEL) stations in this region show that greater than 60% of annual precipitation falls as snow during the winter months (Molotch 2009; Serreze et al. 1999). Snowmelt from seasonal snowpacks serves as the primary source of water supply in this region, sustaining as much 50%–75% of the annual flow of the upper Rio Grande basin (Rango 2006). Land cover in the Rio Grande headwaters was composed of 54% forested area (45% evergreen, 8% deciduous, 1% mixed) and 46% nonforested area (33% herbaceous, 4% shrub/scrub, 4% woody wetlands, 1% herbaceous wetlands, 4% barren land, and <1% open water, minimal development, agriculture; Homer et al. 2015; Fig. 1). Bark beetle (BB)-induced tree mortality affected much of the evergreen forested areas in the Rio Grande headwaters beginning around 2000 and plateauing around 2011, resulting in 25% of the basin area (43% of area classified as forested land cover) being affected by BB disturbance (USFS 2016; Fig. 1). Additionally, during the summer of 2013, the West Fork Complex Fire burned in both undisturbed and BB-affected forests, affecting 8% of the area (14% of area classified as
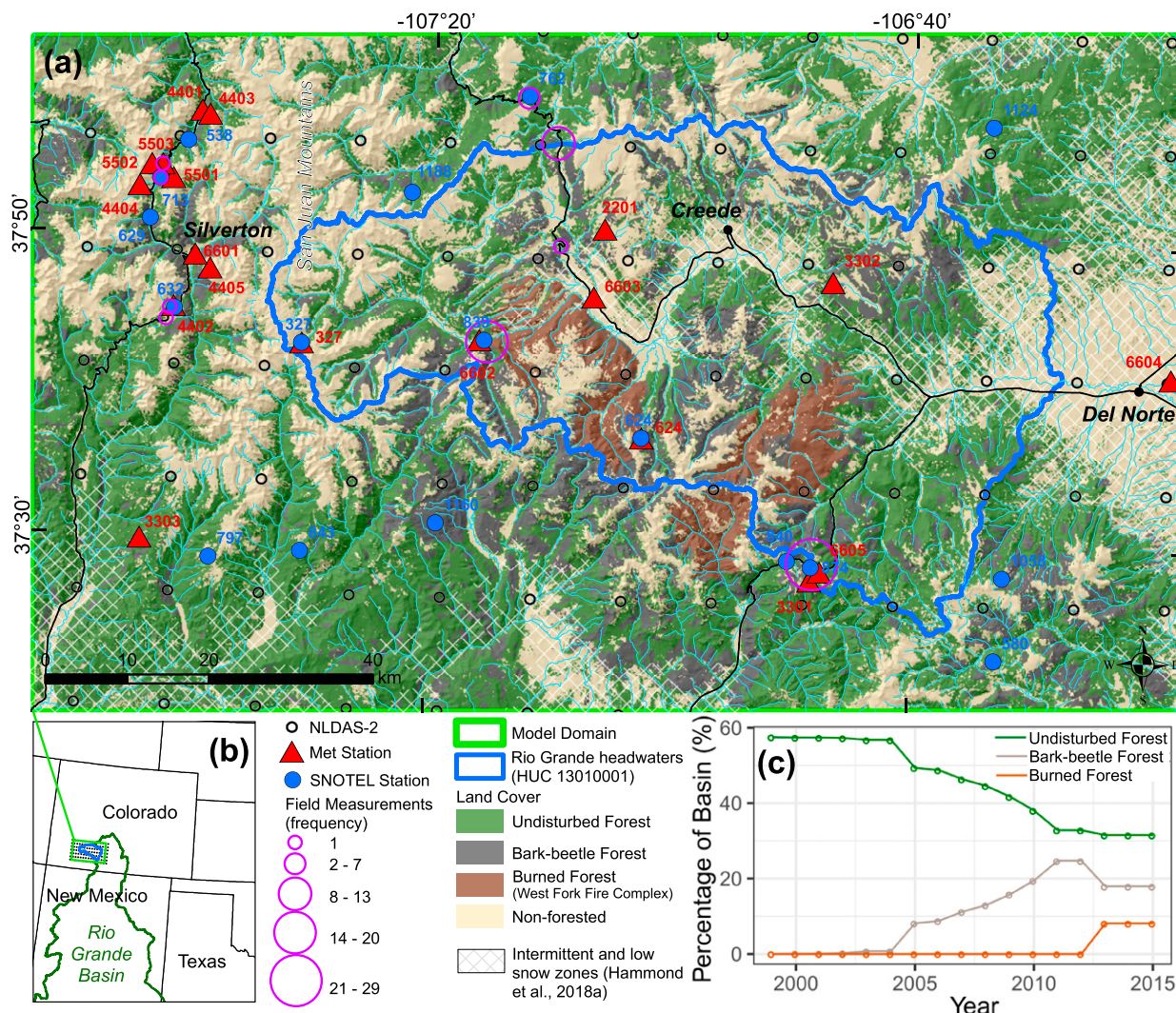
FIG. 1. Study area map showing the (a) model domain and Rio Grande headwaters basin [hydrologic unit code (HUC) 13010001] with land-cover type (Homer et al. 2015; USFS 2016; Eidenshink et al. 2007), snow stations and measurement locations (both used for model evaluation) labeled with a station ID that are defined in Table S1, NLDAS-2 grid centroid locations, and intermittent and low snow zones (Hammond et al. 2018a) highlighted; (b) location of the study area within southwestern Colorado; and (c) time series of the percentage of the Rio Grande headwaters basin composed of forest area, bark beetle disturbance forest area, and burned forest area from wildfire from 1999 to 2015 (Homer et al. 2015; USFS 2016; Eidenshink et al. 2007).

forested land cover) within the Rio Grande headwaters (Fig. 1; https://www.fs.usda.gov/detail/riogrande/home/?cid=stelprdb5425999; Eidenshink et al. 2007).

b. Model description and simulations

To quantify spatial and temporal variations and long-term trends in seasonal snowpack properties across the Rio Grande headwaters (Fig. 1), we ran SnowModel simulations over a 34-yr period from 1984 to 2017. SnowModel is a spatially distributed physically based snow evolution modeling system designed for application in a wide range of environments where snow occurs (Liston and Elder 2006b). SnowModel includes the following submodels: MicroMet (Liston and Elder 2006a), a high-resolution meteorological distribution model;

EnBal (Liston 1995), which computes surface energy exchanges between the snow and atmosphere; SnowPack (Liston and Hall 1995), which simulates the seasonal evolution of snow depth and SWE; SnowTran-3D (Liston and Sturm 1998; Liston et al. 2007), a 3D model that simulates snow redistribution by wind over topographically variable terrain; and SnowAssim (Liston and Hiemstra 2008), a data assimilation system that can be used to assimilate field and remote sensing observations into SnowModel simulations. Required inputs to run SnowModel include temporally varying fields of air temperature T, relative humidity, wind speed and direction, and precipitation P as well as spatially varying fields of topography and land cover. The model uses known relations between meteorological variables and the surrounding topography and land cover to distribute

those variables across the domain. Surface pressure and incoming solar and longwave radiation are additional atmospheric property distributions required to run SnowModel and are computed as part of the MicroMet submodel as described in detail in Liston and Elder (2006a). SnowModel has been rigorously evaluated and shown to perform well in seasonally snow-covered environments similar to the study area (e.g., Greene et al. 1999; Hiemstra et al. 2006; Liston and Elder 2006a,b; Liston et al. 2008; Prasad et al. 2001; Sexstone et al. 2018; Sproles et al. 2013).

SnowModel simulations were run at a 3-hourly time step with a 100-m spatial grid resolution (1.12 million grid cells across the study domain). Elevation, land cover, and canopy cover fraction were provided by the U.S. Geological Survey (USGS) National Elevation Dataset (http://ned.usgs.gov) and National Land Cover Database spatial datasets (https://www.mrlc.gov). The effective leaf area index (LAI*) values across the domain were created by scaling the maximum LAI* for each forest class vegetation type (Table S2 in the online supplemental material) by the canopy cover fraction (e.g., Broxton et al. 2015; Sexstone et al. 2018). This study also implemented dynamic land-cover changes across the simulation time period that were updated each simulation year to represent the temporal effects of BB and wildfire disturbance on snowpack evolution. The cumulative distribution of BB-induced tree mortality from 2000 through 2015 was divided into quantiles representing no mortality, light mortality, moderate mortality, and severe mortality (Bright et al. 2013). Aerial surveys of cumulative BB mortality (USFS 2016) from each year of the simulation time period were used to reduce the spatially variable LAI* across the study domain by 0% (no mortality), 5% (light mortality), 25% (moderate mortality), and 40% (severe mortality) (Bright et al. 2013; Pugh and Gordon 2013; Sexstone et al. 2018). Furthermore, areas subject to wildfire disturbance following the 2013 West Fork Complex Fire (Fig. 1) were prescribed a category of very severe mortality with a LAI* reduction of 82%, which was the difference in LAI* between burned and unburned forest measurements presented by Gleason and Nolin (2016). Deforestation associated with forest management and salvage logging was not considered in this study.

Meteorological forcing data were provided by the 1/8° grid spacing North American Land Data Assimilation System (NLDAS-2) reanalysis forcing dataset (Fig. 1; https://ldas.gsfc.nasa.gov/nldas/; Mitchell et al. 2004; Xia et al. 2012). The NLDAS-2 reanalysis forcing dataset extends back to January 1979; however, given the anomalously wet period in the early 1980s across the region, we began our analysis in 1984 to avoid potential spurious trends (Harpold et al. 2012). Hourly NLDAS-2 T, P, relative humidity, and wind speed and direction data were aggregated to 3-hourly values to correspond with the model simulation time step. The 3-hourly NLDAS-2 forcing data along with mean elevation of each NLDAS-2 grid cell was used by MicroMet to downscale and create the 100-m spatial resolution meteorological forcing data required by SnowModel (e.g., Liston and Elder 2006a; Liston and Hiemstra 2011; Liston et al. 2008; Sexstone et al. 2018) based on Northern Hemisphere monthly lapse rates (refer to Liston and

Elder 2006a) and the 100-m digital elevation model. A 2°C rain/snow threshold air temperature was used in SnowModel for partitioning between rain and snow precipitation (Auer 1974). The SnowAssim data assimilation system (Liston and Hiemstra 2008) was used in this application of SnowModel (e.g., Fletcher et al. 2012; Liston et al. 2008, 2018) to adjust biases in NLDAS-2 winter P forcing data (e.g., Henn et al. 2018; Sexstone et al. 2018). Differences between observed and simulated SWE before peak snow accumulation each year at six long-term SNOTEL stations across the study domain were used to spatially interpolate winter season P adjustment factors for each year of the simulation period (Liston and Hiemstra 2008; Table S3).

This implementation of SnowModel used the snow albedo decay parameterization developed by Gleason and Nolin (2016) to represent snow albedo decay in nonforested, forested, and burned forest areas for both nonmelting and melting snow conditions across the model domain. A threshold of 3 mm of new snow P (3-cm depth of fresh snow with a snow density of 100 kg m^{-3}) was used to reset the simulated snow albedo to its maximum value. Using incoming and outgoing shortwave radiation as well as snow depth observations during the snow-covered period of 2016 and 2017 at two nonforested and two forested stations (Table S4; Fig. 1), we derived the study area-specific albedo decay gradient parameters based on the mean of best-fit exponential regression functions between the days since snowfall and the snow albedo (Table S4, Fig. S1; Gleason and Nolin 2016). All albedo decay parameters for burned forested areas as well as the maximum and minimum snow albedo for forested and open areas presented by Gleason and Nolin (2016) were additionally used in this study (Table S4, Fig. S1). This study was not able to directly incorporate the time-varying influence of light-adsorbing particles (LAPs) such as dust and black carbon on snow albedo (Gleason et al. 2019; Skiles et al. 2018) into the model simulations because historical data were not available for the entire simulation period (e.g., Painter et al. 2012). However, the albedo parameters used in this study were derived from 2016 and 2017, which were considered "average" dust-on-snow years in the Rio Grande headwaters (http://www.codos.org/#dust-enhanced-runoff-classification); therefore, the model simulations are likely to represent the mean influence of LAPs on snow albedo over the time period, but not its interannual variability.

c. Model evaluation

This study used a combination of station observations, field measurements, and remote sensing observations to provide a thorough evaluation and error analysis of the SnowModel simulations. All model evaluation performance statistics were computed ("hydroGOF" R package; Zambrano-Bigiarini 2017) based on daily values using the coefficient of determination (R^2), root-mean-square error (RMSE), and mean bias for daily variables or percent bias (PBias) for cumulative variables. Additionally, linear regression trends were computed (R Core Team 2019) for observed and simulated values, and a statistical comparison of both the linear regression slopes and linear regression intercepts was computed by analysis of covariance (ANCOVA). A probability

TABLE 2. Mean summary values of model simulation performance statistics based on the comparison of daily SnowModel simulation values with daily station observations for water years 2016 and 2017. Bolded R^2 values denote all p values < 0.01.

Variable	No. of stations	R^2	Bias	RMSE
Air temperature (°C)	33	**0.95**	−0.3	2.0
Relative humidity (%)	13	**0.74**	0.46	11
Vapor pressure (Pa)	13	**0.89**	4.7	59
Wind speed (m s^{-1})	10	**0.50**	0.4	2.4
Incoming shortwave radiation (W m^{-2})	6	**0.60**	−0.4	59
Net radiation[a] (W m^{-2})	3	**0.33**	−8.6	29
Albedo[a]	5	**0.36**	−0.01	0.17
Cumulative precipitation assimilation stations[b] (mm)	6	**0.99**	10%	77
Cumulative precipitation[b] (mm)	11	**0.98**	15%	94
SWE assimilation stations[b] (mm)	6	**0.89**	6%	96
Snow water equivalent[b] (mm)	11	**0.78**	11%	93

[a] Denotes that the simulation and observation comparisons were only made during the snow-covered period.
[b] Denotes that the model simulation performance statistics are based on the entire period of record (water years 1984 through 2017) and that the percent bias rather than mean bias is presented.

(p) value < 0.05 for the coefficient of determination and ANCOVA were considered statistically significant in this study.

1) STATION OBSERVATIONS

Daily mean observations from 34 meteorological stations within the model domain during the 2016 and 2017 water years were used to evaluate simulated meteorological forcing (Fig. 1; Table S1). Station observations were used to evaluate simulated T, relative humidity, vapor pressure, wind speed, net radiation, incoming shortwave radiation, and albedo (Table S1). Furthermore, daily observations of P and SWE at 17 SNOTEL stations were used to assess the performance of the simulated P and snow mass balance over the entire model simulation period (1984–2017); these evaluations were completed separately for SNOTEL stations used for data assimilation ($n = 6$; assimilation stations) and not used for data assimilation ($n = 11$; evaluation stations). Simulated SWE values equal to zero were not included to calculate evaluation metrics (Table S1). All land-cover grids (100 m) that overlapped SNOTEL station locations were classified as forested areas by the national land cover database. Given that SWE measurements at SNOTEL stations are located in small sheltered forest openings, this study disabled snow interception by the forest canopy for these overlapping 100-m grid cells. This allowed the SNOTEL-associated grid cells to represent canopy snow interactions without the influence of snow interception and the corresponding canopy-intercepted sublimation losses (i.e., small forest gap; Ellis et al. 2013) and provided a more reasonable comparison between the simulated and observed values at grid cells that overlapped SNOTEL stations.

2) FIELD MEASUREMENTS

Field snow surveys were conducted in 2016 and 2017 at 73 locations within the study area (Fig. 1) to measure snow properties in both forested and nonforested locations. At each field measurement location ($n = 73$), nine snow depth measurements were collected using a snow depth probe across a 20 m × 20 m grid and a mean determined for each location.

At 46 of the measurement locations, snow density was measured using either a Federal snow sampling tube (Kinar and Pomeroy 2015) or snowpit observations using a 250-cm^3 snow density wedge cutter (Kinar and Pomeroy 2015), and SWE was computed based on the mean snow depth × snow density. Field measurements were directly compared to simulated snow depth and SWE at grid cells that overlapped the field measurement locations on each date. Field snow survey data are available in Sexstone (2020).

3) REMOTE SENSING OBSERVATIONS

Simulated SCA between 2000 and 2017 was evaluated using remotely sensed MODIS SCA data from the MOD10A2 product (https://nsidc.org/data/mod10a2). The 8-day MODIS SCA product was used in favor of the daily MODIS SCA product to minimize the influence of cloud coverage on the model evaluation of snow-cover duration. Model grid cells were classified as snow covered if the simulated SWE was greater than 10 mm on the same day (Gascoin et al. 2013). The MOD10A2 maximum SCA across the model domain (observed by MODIS for every 8-day period) was compared to the maximum SCA simulated by SnowModel during the same period.

Simulated SWE across the Rio Grande headwaters was also evaluated using the National Aeronautics and Space Administration (NASA) Jet Propulsion Laboratory (JPL) Airborne Snow Observatory (ASO) dataset that was collected near peak snow accumulation in the basin on 3 April 2016 (Painter 2018; https://nsidc.org/data/ASO_50 M_SWE/versions/1). ASO performs airborne surveys to estimate snow depths at a 3-m resolution by differencing snow-off from snow-on elevations obtained from lidar (Painter et al. 2016). The ASO SWE product is then derived at a 50-m spatial resolution by combining the ASO snow depths with simulated snow density fields (Hedrick et al. 2018; Painter et al. 2016). We resampled the 50-m ASO SWE dataset to the 100-m SnowModel grid and directly compared it to the SnowModel SWE simulated on 3 April 2016.
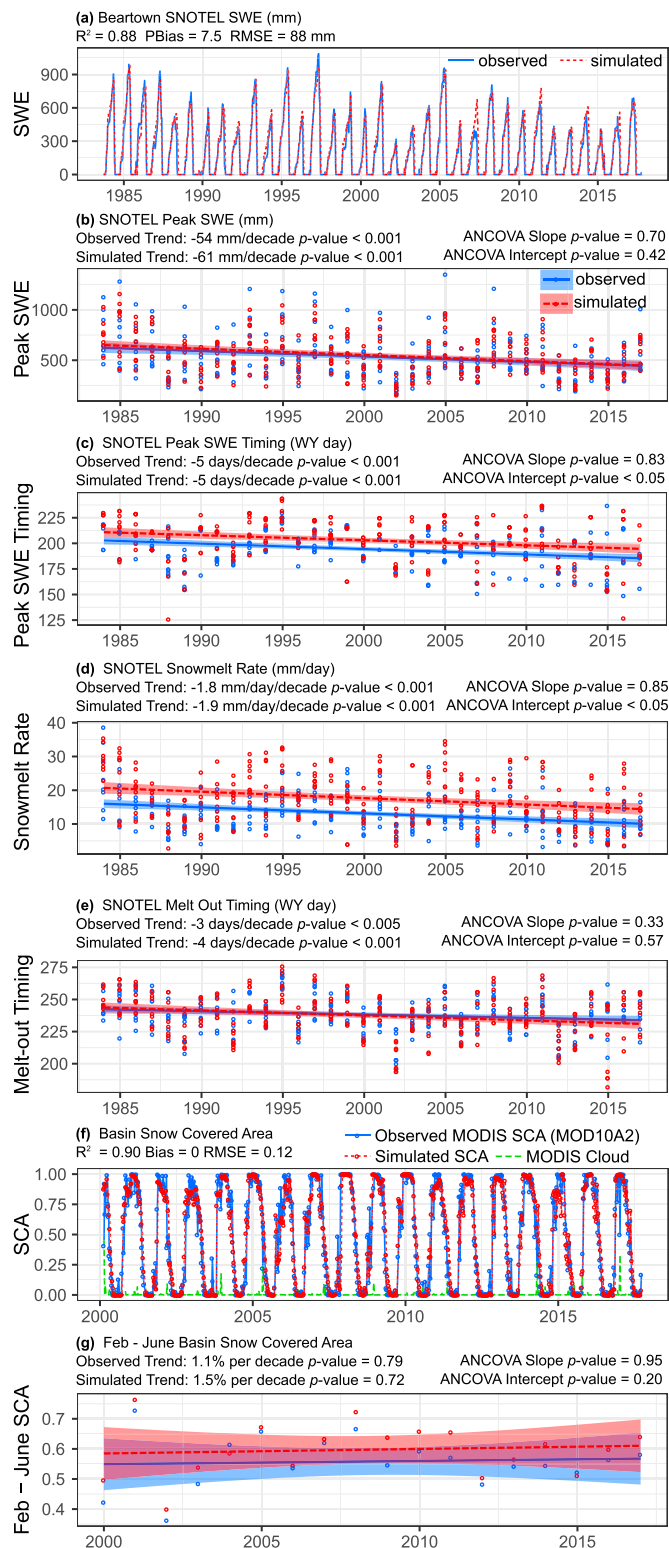
FIG. 2. Time series plots and model evaluation statistics of (a) daily observed SNOTEL SWE compared to daily simulated SWE at Beartown (station ID 327); annual observed SWE metrics compared to annual simulated SWE metrics at eight long-term SNOTEL locations for (b) peak SWE, (c) peak SWE timing, (d) snowmelt rate, and

d. Trend analyses

The 3-hourly SnowModel outputs were aggregated to daily values over the simulation time period. Furthermore, annual [water year (WY); 1 October–30 September] variables representing climate and snowpack conditions (i.e., climate and snow metrics) for each grid cell within the model domain were computed for spatiotemporal analyses. Annual climate and snow metrics that were evaluated in this study are described in Table 1. For each metric (Table 1), the nonparametric Mann–Kendall test (Mann 1945) and the Theil–Sen slope estimator (Sen 1968) were used to evaluate trends for each grid cell across the model domain ("rkt" R package; Marchetto 2017). A p value < 0.05 for the Mann–Kendall test was considered statistically significant in this study. Trend statistics were evaluated based on elevation, aspect, and land-cover type within the basin. Model output data that support the findings of this study are available in Sexstone (2020).

3. Results

a. Model evaluation

1) STATION OBSERVATIONS

Daily mean simulated T was significantly related (all p values < 0.01) with daily mean T observations and showed a small negative mean bias with station observations during water years 2016 and 2017 (Table 2). Simulated relative humidity and vapor pressure were also significantly related with observations (mean $R^2 = 0.74$ and 0.89, respectively; all p values < 0.01) and showed minimal mean bias with station observations across the domain, indicating the model was able to reasonably represent atmospheric moisture conditions (Table 2). Simulated wind speeds were modestly, but significantly, related with observations (mean $R^2 = 0.50$; all p values < 0.01), with the lowest errors observed at the highest elevations (Fig. S2). Simulated incoming shortwave radiation was also modestly related with observations (mean $R^2 = 0.60$; all p values < 0.01) and showed a very small mean bias (Table 2). During the snow-covered periods of water years 2016 and 2017, both simulated net radiation and albedo were modestly correlated with observations (Table 2), with a mean RMSE of 29 W m^{-2} and 0.17, respectively (Table 2).

Over the entire simulation period (water years 1984–2017), simulated cumulative P at SNOTEL stations both used for data assimilation ($n = 6$; assimilation stations) and not ($n = 11$; evaluation stations) were highly correlated with observations (mean $R^2 = 0.99$ and 0.98, respectively; all p values < 0.01) and were biased slightly high with a mean PBias of 10% and

15%, respectively (Table 2). Likewise, simulated SWE at assimilation and evaluation stations were well correlated with observations (Table 2; Fig. 2) and exhibited a mean RMSE of 96 and 93 mm, respectively, for all time periods when the simulated SWE was greater than zero. Errors in simulated P and SWE were not strongly related to station elevation (Fig. S3). The time series of simulated and observed SWE for SNOTEL stations available over the entire simulation period of record ($n = 8$) was used to compare the long-term trends in annual peak SWE, peak SWE timing, snowmelt rate, and melt-out timing (Fig. 2). An ANCOVA analysis between the linear regression slopes of these annual metrics showed no significant difference (all p values > 0.05) between the simulated and observed values (Fig. 2). Additionally, an ANCOVA analysis of the linear regression intercept values showed no significant difference between both simulated and observed peak SWE and melt-out timing (Fig. 2). However, both simulated and observed peak SWE timing and snowmelt rate intercepts were significantly different (p values < 0.05), highlighting a positive but temporally consistent annual bias in both metrics (Fig. 2).

2) FIELD MEASUREMENTS

Simulated SWE and snow depth were highly related with field observations collected across the study area ($R^2 = 0.82$ and 0.73, respectively; p values < 0.001; Fig. 3). However, both simulated SWE and snow depth were biased slightly low compared to observations with a mean PBias of about -16% and -21%, and an RMSE of 166 mm and 0.44 m, respectively (Fig. 3). Systematic errors between different land-cover types were not observed when comparing field snow observations to the SnowModel simulations (Fig. 3).

3) REMOTE SENSING OBSERVATIONS

Simulated snow-cover duration across the model domain was highly related to MODIS SCA observations ($R^2 = 0.90$; p value < 0.001; Fig. 2) during the period of record (water years 2000 through 2017) when the simulated SCA was greater than zero, and the observed MODIS cloud coverage was less than 5% of the model domain (Fig. 2). The mean bias of the simulated SCA was equal to zero and the RMSE was 0.12 when compared to MODIS observations (Fig. 2). However, an evaluation of the annual mean SCA from February through June showed a slightly positive bias in simulated SCA (Fig. 2). An ANCOVA analysis between the linear regression trend slopes for the simulated and observed mean February through June SCA showed no significant difference (p value > 0.05; Fig. 2).

On 3 April 2016, the basinwide mean value and standard deviation of simulated SnowModel SWE (238 ± 216 mm)

←

(e) melt-out timing; (f) observed MODIS 8-day maximum snow covered area (SCA) compared to simulated 8-day maximum SCA for the MODIS period of record; and (g) observed MODIS annual February–June mean SCA compared to simulated February–June mean SCA for the MODIS period of record.
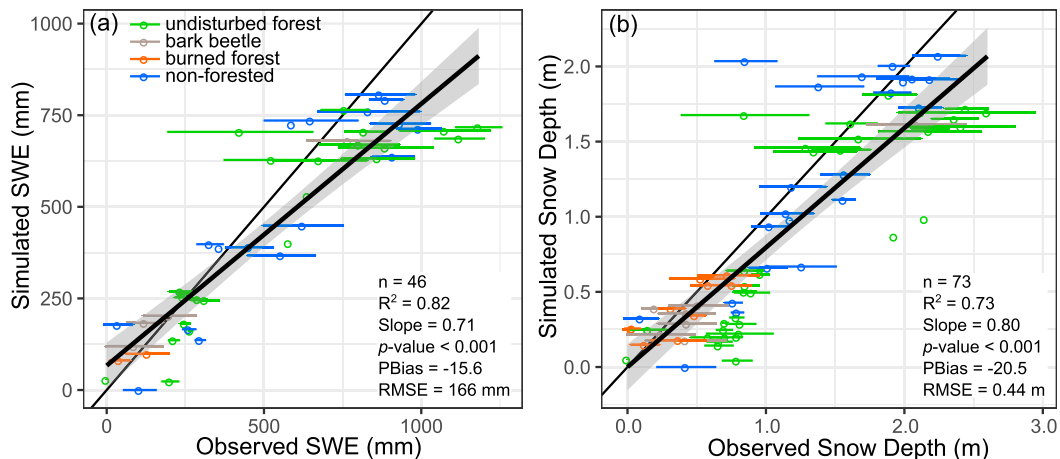
FIG. 3. Relation between the observed (field measurements) and simulated (a) SWE and (b) snow depth with the standard deviation of grid field measurements denoted with error bars and the land-cover type denoted by color. The thick black line and surrounding gray shading shows the linear regression trendline and 95% confidence interval. The thin black line represents the 1:1 line.

compared well to the ASO SWE estimates (202 ± 226 mm). The mean difference between the SnowModel SWE and ASO-derived SWE across the basin was 36 mm, highlighting a slight positive PBias (18%) in the model simulations (Fig. 4). This positive bias was consistent across all elevation zones that contained substantial volumetric SWE (Fig. 4). A grid-to-grid comparison of the SnowModel and ASO-derived SWE showed a significant relation (*p* value < 0.001) with a comparable linear regression slope, absolute PBias, and RMSE to that calculated from field measurements (Figs. 3 and 4).

b. Trends in winter T and P

Statistically significant trends (hereafter referred to as "trends") of increasing simulated mean winter *T* and decreasing simulated winter *P* were observed within the study area. However, these trends were spatially variable and only occurred in 30% of the Rio Grande headwaters (Table 3; Fig. 5). Simulated winter *T* showed upward trends of approximately $0.3°\text{C decade}^{-1}$ (Table 3) with the high elevations covering the greatest percentage of area relative to the total elevation zone area (relative percentage) with trends (Table 3; Fig. 5). Simulated winter *P* showed downward trends that increased in magnitude with elevation from -35 to $-76 \text{ mm decade}^{-1}$ (Table 3). Downward trends in simulated snowfall were also comparable to simulated winter *P*; however, the lowest elevations covered the greatest relative percentage of area with trends (Table 3).

c. Trends in snow accumulation

Downward trends in simulated peak SWE were similar in magnitude to trends in simulated winter *P* and snowfall (Table 3) and covered a similar percentage of the Rio Grande headwaters as downward snowfall trends (51% compared to 62%). The downward trend slopes in simulated peak SWE increased in magnitude from low to high elevation (Table 3; Fig. 6). However, the middle elevations covered the greatest relative percentage of area with trends. These middle elevations were coincident with

the greatest simulated volumetric peak SWE (i.e., volume of water stored as snow) across the Rio Grande headwaters (Figs. 6e,f). Furthermore, south-facing aspects in the middle and high elevations had a greater relative percentage of area with significant trends in simulated peak SWE than comparable north-facing aspects (Fig. 7). Downward trends in simulated SWE:*P* (Table 1) on the order of $-0.04 \text{ decade}^{-1}$ occurred across 48% of the basin. The largest magnitude downward trends in simulated SWE:*P* occurred within the low elevations; however, the middle and high elevations covered a greater relative percentage of area with trends (Table 3). In contrast, the largest relative percentage of area with downward trends in simulated peak SWE timing occurred in the low and middle elevations with the greatest magnitude trends on the order of $-11 \text{ days decade}^{-1}$ occurring in the middle elevations (Table 3). Downward trends in simulated number of snow-covered days were widespread, with significant trends covering 48% of the Rio Grande headwaters, and increased in magnitude from high to low elevation (Table 3).

The spatial variability of trends in simulated snow accumulation was also dependent on land-cover type and disturbance. Mean simulated peak SWE was generally greater in non-forested areas compared to forested areas across most elevations, although mean simulated volumetric SWE was greatest in forested areas across the middle elevations because these areas accounted for a greater surface area within the domain (Fig. 6). Downward trend slopes of simulated peak SWE were similar in magnitude between different land-cover types and disturbances for most elevations (Fig. 6). Nonforested areas generally had the highest relative percentage of downward trends in simulated peak SWE whereas disturbed forest areas from BB and wildfire showed the lowest relative percentage (Fig. 6).

d. Trends in snowmelt

Downward trends in simulated total snowmelt quantity (Table 1) were also widespread across the study area and
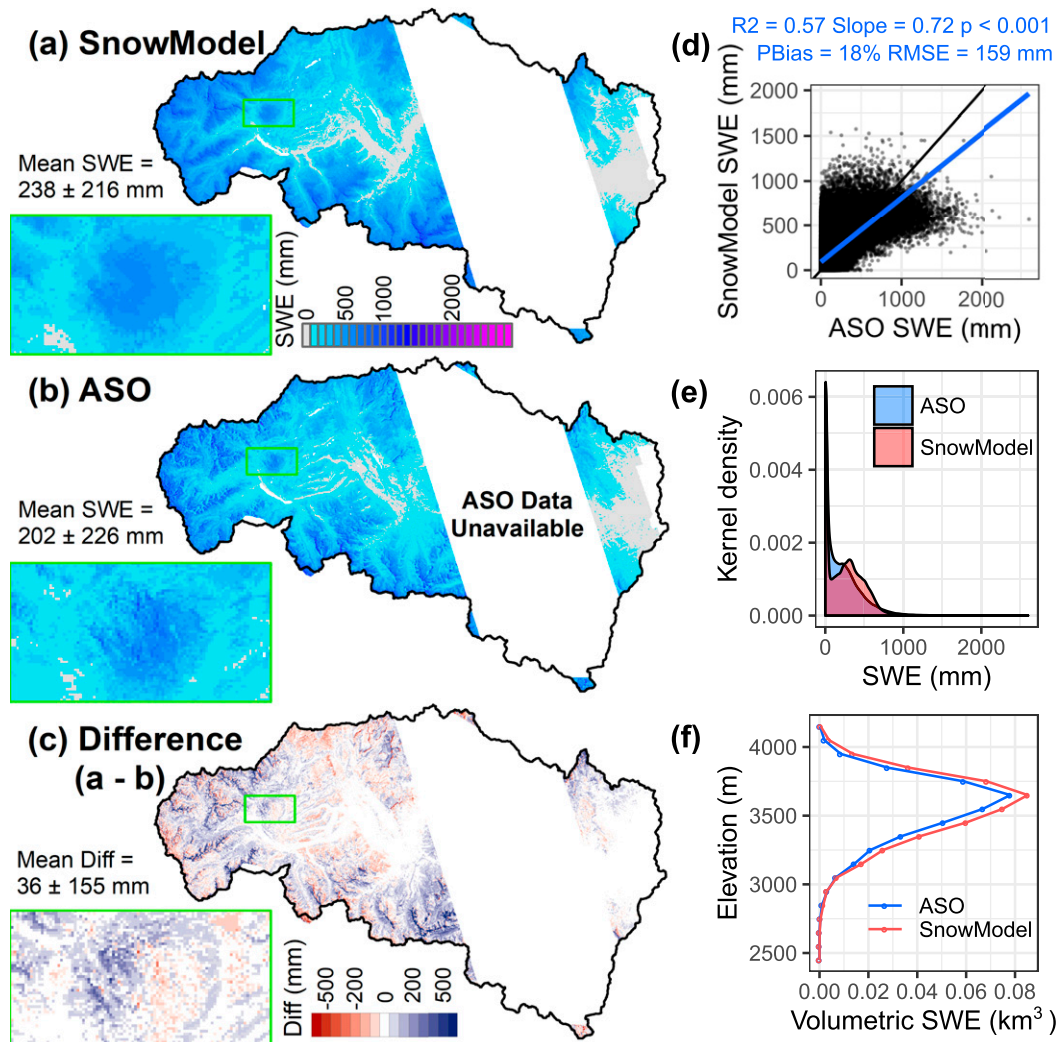
FIG. 4. Spatial distribution of SWE across the Rio Grande headwaters (a) simulated by SnowModel and (b) observed by Airborne Snow Observatory (ASO) on 3 Apr 2016, and (c) the difference (Diff) [(a) − (b)] in SWE between SnowModel and ASO. A comparison between the simulated SnowModel and observed ASO SWE is shown by the (d) linear regression relation, (e) kernel density distribution comparison, and (f) comparison of volumetric SWE within 100-m elevation zones (North American Vertical Datum of 1988).

covered over 57% of the Rio Grande headwaters with a mean trend slope of −56 mm decade^{-1}. Trend slopes and the relative percentage of area with trends increased from low to high elevations (Table 3). Simulated snowmelt rate also decreased over the study period on the order of −2.3 mm day^{-1} decade^{-1}, although downward trends predominantly covered the middle elevations (Table 3; Fig. 8). Within these middle elevations, downward trends in snowmelt rate were greater in south-facing compared to north-facing aspects (Fig. 7). Downward trends in simulated SM50 (Table 1; mean of −8 days decade^{-1}) covered 51% of the basin. The largest magnitude downward trends in simulated SM50 occurred within the low and middle elevations especially on south-facing aspects (Table 3; Fig. 7), and the middle elevations covered the greatest relative percentage of area with trends (Table 3; Fig. 9). Simulated melt-out timing showed similar

trends and elevational differences as that of SM50 with the largest magnitude trends within the low elevations (Table 3).

Mean simulated snowmelt rate and downward trends in simulated snowmelt rate were generally greater in nonforested compared to forested areas (Fig. 8). Additionally, nonforested areas generally covered the greatest relative percentage of area with trends in snowmelt rate in the low to middle elevations, whereas forested areas covered the greatest relative percentage in middle to high elevations (Fig. 8). All forested areas exhibited similar trends and spatial patterns in simulated snowmelt rate, although undisturbed forests had slightly greater magnitude trend slopes and relative percentage of area with trends in simulated snowmelt rate compared to disturbed forest areas from BB and wildfire (Fig. 8). Mean simulated SM50 was greater (i.e., later in the year) in nonforested compared to forested areas

TABLE 3. Simulated climate and snow metrics mean, standard deviation (SD), trend slope, and relative basin area percentage of statistically significant trends for the low elevations, middle elevations, and high elevations across the Rio Grande headwaters. Trend slope mean is the mean of all statistically significant trend slopes (p value < 0.05).

Climate/snow metric	Low elevations (2400–3000 m)	Middle elevations (3000–3600 m)	High elevations (3600–4200 m)
Snow metric mean ($\pm$ SD)			
Winter T (°C)	-0.7 ± 0.8	-3.5 ± 0.9	-5.8 ± 0.6
Winter P (mm)	322 ± 99	624 ± 178	913 ± 175
Snowfall (mm)	227 ± 86	555 ± 177	898 ± 183
Peak SWE (mm)	103 ± 65	330 ± 167	709 ± 213
SWE:P (mm^{-1})	0.29 ± 0.12	0.49 ± 0.14	0.76 ± 0.13
Peak SWE timing (WY day)	148 ± 21	191 ± 19	224 ± 10
Snow-covered days (days)	103 ± 37	186 ± 31	251 ± 18
Total snowmelt (mm)	134 ± 74	369 ± 170	741 ± 229
Snowmelt rate (mm day^{-1})	5.1 ± 2.1	11.3 ± 4.3	18.2 ± 3.2
SM50 (WY day)	165 ± 23	215 ± 20	254 ± 12
Melt-out timing (WY day)	173 ± 24	225 ± 21	267 ± 13
Sublimation (mm)	77 ± 43	185 ± 58	188 ± 56
Effective sublimation (mm^{-1})	0.24 ± 0.1	0.31 ± 0.09	0.22 ± 0.07
Trend slope mean (relative basin area percentage of statistical significance)			
Winter T (°C decade^{-1})	0.34 (9)	0.34 (33)	0.30 (52)
Winter P (mm decade^{-1})	-35 (34)	-56 (32)	-76 (16)
Snowfall (mm decade^{-1})	-29 (88)	-52 (59)	-77 (25)
Peak SWE (mm decade^{-1})	-35 (17)	-54 (64)	-77 (58)
SWE:P (mm^{-1} decade^{-1})	-0.05 (8)	-0.04 (61)	-0.03 (72)
Peak SWE timing (WY day decade^{-1})	-9 (33)	-11 (48)	-8 (5)
Snow-covered days (days decade^{-1})	-15 (52)	-13 (39)	-9 (75)
Total snowmelt (mm decade^{-1})	-29 (50)	-53 (55)	-94 (80)
Snowmelt rate (mm day^{-1} decade^{-1})	-1.7 (7)	-2.4 (42)	-2.6 (5)
SM50 (WY day decade^{-1})	-9 (45)	-8 (58)	-5 (31)
Melt-out timing (WY day decade^{-1})	-9 (52)	-8 (51)	-6 (46)
Sublimation (mm decade^{-1})	-9 (85)	-18 (53)	-19 (3)
Effective sublimation (mm^{-1} decade^{-1})	-0.03 (1)	0.01 (2)	0.02 (34)

(Fig. 9). In nonforested areas, the greatest magnitude downward trends and highest relative percentage of area with significant trends in SM50 covered the low elevations, whereas in forested areas these were found in the middle and high elevations (Fig. 9). Forests disturbed from wildfire covered the greatest relative percentage of area with downward trends in SM50 (Fig. 9).

e. Trends in snow sublimation

Downward trends in simulated snow sublimation (Table 1) covered over 54% of the Rio Grande headwaters with a mean trend slope of -14 mm decade^{-1}. For areas below tree line, the downward trend slopes in simulated snow sublimation increased in magnitude with increasing elevation (Table 3; Fig. 10). However, the relative percentage of area covered with trends decreased from low to high elevations (Table 3; Fig. 10). Both downward simulated snow sublimation trend magnitude and the relative percentage of area covered with trends were generally greater on north-facing compared to south-facing aspects (Fig. 7). Additionally, similar to simulated peak SWE, the middle elevations were coincident with the greatest simulated volumetric snow sublimation amounts across the Rio Grande headwaters (Fig. 10). In contrast to simulated snow sublimation, upward trends in simulated effective sublimation (Table 1) of 0.02 decade^{-1} covered 7% of the basin.

The low and middle elevations exhibited few trends in simulated effective sublimation. However, significant upward trends in simulated effective sublimation covered 34% of the high-elevation alpine areas in the Rio Grande headwaters (Table 3).

Mean simulated snow sublimation was generally much greater in forested areas compared to nonforested areas, and the mean simulated volumetric snow sublimation was greatest in middle elevation forested areas (Fig. 10). Downward trend slopes of snow sublimation and the relative percentage of area covered with trends were also greater in magnitude in forested compared to nonforested areas (Fig. 10). Additionally, within forested areas, trend magnitudes and the relative percentage of area with trends increased from undisturbed forests to bark beetle disturbances to wildfire disturbances (Fig. 10).

4. Discussion

a. Spatial variability of snowpack trends

Key results of this study highlight how trends in simulated snow metrics across the Rio Grande headwaters exhibited widespread declines between 1984 and 2017, but also varied spatially depending on elevation, aspect, and land cover.
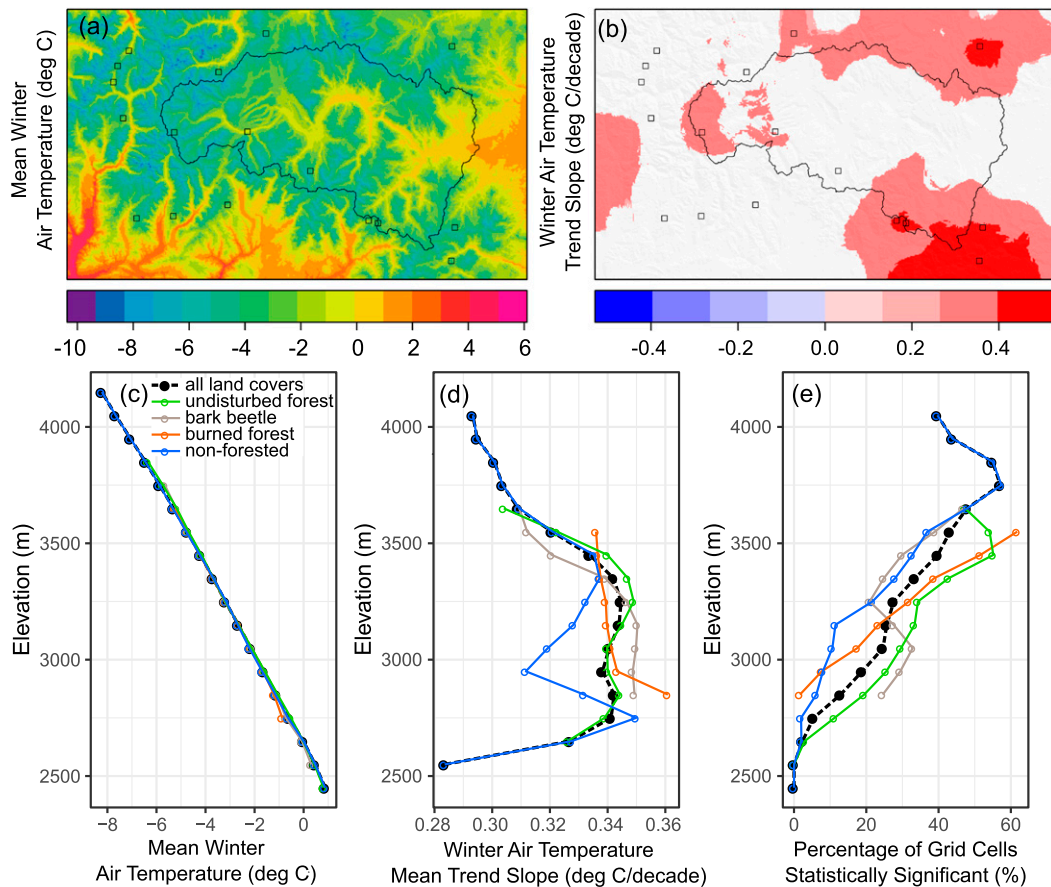
FIG. 5. Map of simulated (a) mean (1984–2017) winter air temperature in degrees Celsius (°C) and (b) statistically significant (*p* value < 0.05) trend slopes in winter air temperature across the model domain (white areas are not statistically significant) with (c) mean winter air temperature, (d) statistically significant winter air temperature trend slope, and (e) percentage of grid cells that are statistically significant summarized for the Rio Grande headwaters by both elevation zone (100-m increments in North American Vertical Datum of 1988) and land-cover type. The squares in (a) and (b) show the locations of SNOTEL stations within the model domain.

Trends did not occur everywhere within the basin, and some areas were more sensitive than others with distinct differences between snow metrics. Elevation was found to be an especially important variable related to trends in snow metrics across the basin scale, consistent with recent modeling studies in the Sierra Nevada, California, United States (Musselman et al. 2017a) and the Pyrenees, Spain and France (López-Moreno et al. 2020), highlighting elevation as an important indicator of snowpack sensitivity to changing climate. Elevation can exert a strong control on the relative importance of *P* and *T* to changes in snow properties (Morán-Tejeda et al. 2013; Hammond et al. 2018b). In this study, we observe elevation-dependent trends in *T* and *P* that cause an elevation dependence in peak SWE trends with middle elevations exhibiting the largest relative surface areas with significant reductions in SWE. This result is somewhat counterintuitive to the expectation that snowpack declines will be most widespread in the low elevations zones. However, López-Moreno et al. (2020) highlighted similar results showing declining SWE trends at high elevations and no trend at low elevations as a result of recent warming in the fall

and spring months having a greater influence on persistent snowpacks with a longer snow-cover duration. Further to this point, downward trends in simulated total snowmelt quantity were greatest and most widespread at the highest elevations (Table 3; Fig. 8). This indicates late season snow accumulation following peak SWE, which can be substantial in high-elevation areas, may have had pronounced decreases at the highest elevations. Similar to peak SWE, we also highlight that the greatest relative percentage of trends in snowmelt rate were most pronounced in the middle elevations of the study area. Decreasing snowmelt rates presented in this study are a result of the contraction of the snowmelt season (e.g., downward trends in peak SWE timing, SM50, and melt-out timing; Table 3) to a period of lower available energy and are consistent with the observational and modeling study presented by Musselman et al. (2017b). Furthermore, our results show the area with the greatest volumetric snow water storage is also the area with the greatest relative percentage of downward snowmelt rate trends (i.e., middle elevations), which is consistent with
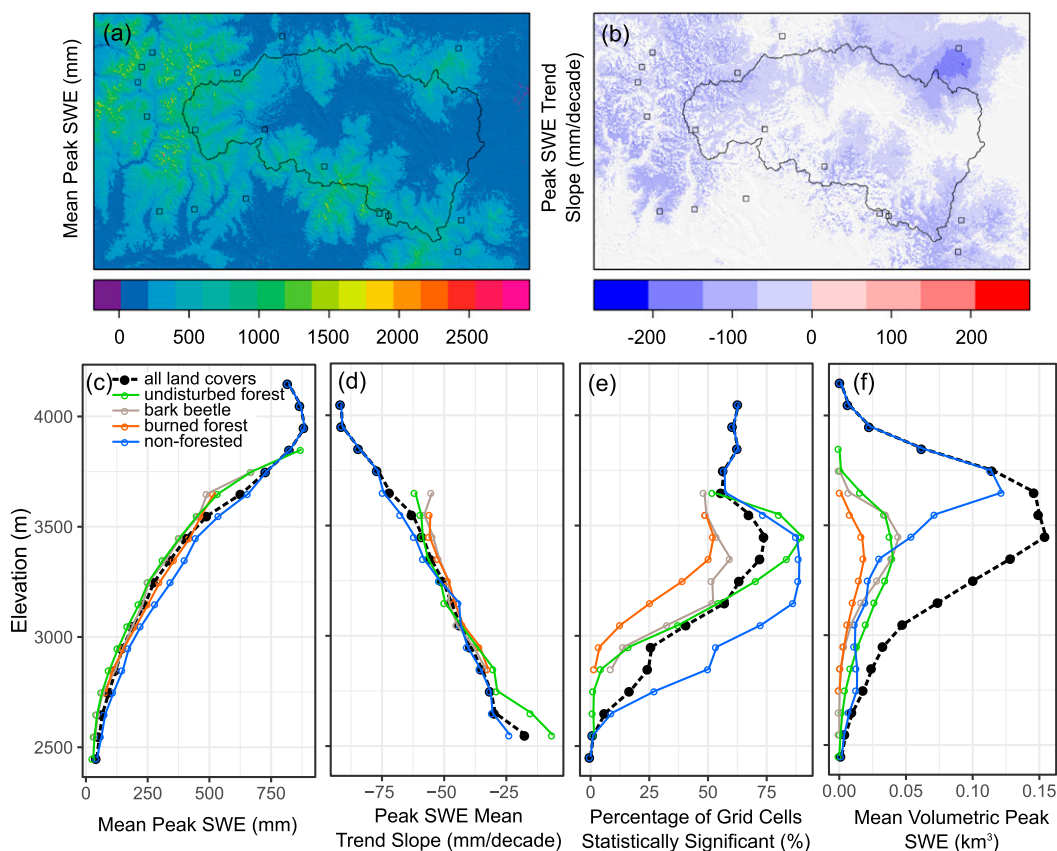
FIG. 6. Map of simulated (a) mean (1984–2017) peak snow water equivalent (SWE) and (b) statistically significant (*p* value < 0.05) trend slopes in peak SWE across the model domain (white areas are not statistically significant) with (c) mean peak SWE, (d) statistically significant peak SWE trend slope, (e) percentage of grid cells that are statistically significant, and (f) mean volumetric peak SWE summarized for the Rio Grande headwaters by both elevation zone (100-m increments in North American Vertical Datum of 1988) and land-cover type. The squares in (a) and (b) show the locations of SNOTEL stations within the model domain.

recent climate change snow sensitivity experiments presented by Musselman et al. (2017a).

Land cover was also found to be an important variable related to trends in snow metrics across the basin scale. Snowmelt rate trends in middle elevations varied substantially between areas, with downward trends generally greater in magnitude in nonforested areas compared to forested areas (Fig. 8). Furthermore, nonforested areas generally had a higher relative percentage of downward trends in simulated peak SWE compared to forested areas (Fig. 6). Although longwave emissivity from trees is enhanced under a warming climate, nonforested areas may have had more widespread downward trends in peak SWE as a result of SWE reductions in forested areas being buffered by downward trends in snow sublimation (Fig. 10). It has been indicated that sublimation processes may have an important influence on snowpack sensitivity to changing climate conditions (Harpold et al. 2012; Harpold and Brooks 2018; López-Moreno et al. 2017; Sexstone et al. 2018). Below tree line in the study area, downward trends in simulated sublimation were a result of reductions in both surface and canopy sublimation components but were most prevalent in

forested areas as a result of canopy sublimation decreases (Table 3; Fig. 10). Furthermore, forest disturbances were shown to substantially magnify downward snow sublimation trends (Fig. 10). These trend results are consistent with the forest disturbance and climate change simulations presented in Sexstone et al. (2018) highlighting decreases in snow sublimation as a result of reductions in both canopy-intercepted snow and overall snow-cover duration despite increases in subcanopy wind exposure and radiation simulated by the model. Interestingly, alpine areas above tree line generally showed increases in blowing snow sublimation but decreases in surface sublimation components resulting in a very small percentage of area covered with trends (Fig. 10). However, significant increases in effective sublimation covered 34% of high-elevation areas (Table 3). Upward trends in effective sublimation associated with decreasing snow amounts is consistent with previous research highlighting an increased importance of snow sublimation in low snow years (Reba et al. 2012; Sexstone et al. 2016, 2018). Given the importance of snow sublimation to the snow mass balance in alpine areas (e.g., Gascoin et al. 2013; Knowles et al. 2015; MacDonald et al. 2010;
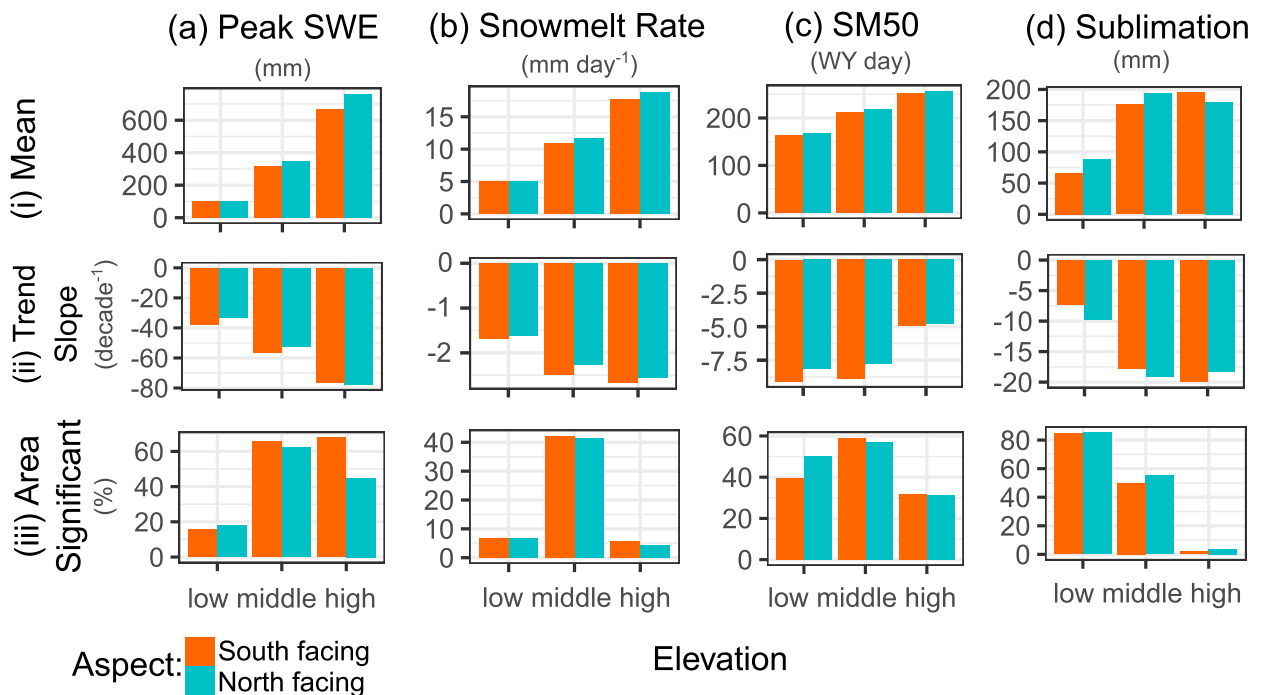
FIG. 7. Summary of snow metric (i) mean value, (ii) statistically significant trend slope (p value < 0.05), (iii) and percentage of grid cells (area) that are statistically significant summarized for the Rio Grande headwaters for south-facing and north-facing aspects within elevation ranges (North American Vertical Datum of 1988) of low (2400–3000 m), middle (3000–3600 m), and high (3600–4200 m). Snow metric summaries include: (a) peak SWE, (b) snowmelt rate, (c) SM50, and (d) snow sublimation. Refer to Table 1 for snow metrics definitions.

Sexstone et al. 2018), future work is needed to evaluate how blowing snow sublimation losses may respond to changes in climate in alpine areas.

b. Basinwide snowpack trends

The results from this study can be used to provide important context to how snowpacks are changing or are projected to change in the future at the basin scale. To put our results in context with previous investigations, we normalized the mean snow metric trends across the study basin by the basin mean of the snow metric for areas with trends over the period of analysis (1984–2017), yielding an estimate of percentage change decade^{-1} (Fig. 11). These results highlight that snowmelt rate, peak SWE, and total snowmelt amount displayed the greatest percentage change in this study (Fig. 11). Snowmelt rate decreased by 20% decade^{-1}, and total snowmelt amount decreased by 13% decade^{-1}. These trends are greater in magnitude than the climate sensitivity analysis of -10% °C^{-1} in total snowmelt presented by Musselman et al. (2017a). Given our results of upward trends in T of 0.3°C decade^{-1}, this comparison highlights the importance that changes in winter P had in snowpack trends presented in this and other studies (e.g., Hammond et al. 2018b; Morán-Tejeda et al. 2013; Zeng et al. 2018). The time period analyzed in this study was coincident with wetter decades in the 1980s and 1990s with intermittent drought conditions in the 2000s and 2010s in the upper Rio Grande basin (Lehner et al. 2017). These drought conditions (-52 mm decade^{-1} in winter P

across the study area) and upward trends in T (0.3°C decade^{-1} winter T across the study area) combined to influence snowpack changes over the study period. Peak SWE decreased by 14% decade^{-1} in the current study. Our peak SWE trend results are slightly more pronounced than those presented by Zeng et al. (2018) of -12% decade^{-1} (1982–2016) for snowy areas across the western United States and an analysis of SNOTEL station trends in the upper Rio Grande basin showing -10% decade^{-1} (1984–2009) by Harpold et al. (2012). Additionally, a recent study by Chavarria and Gutzler (2018) showed decreases in 1 April SWE at snow courses in the Rio Grande headwaters by 25% from 1958 to 2015 (4% decade^{-1}). Differences arising from varying study periods highlight the strong snowpack sensitivity to hydroclimate changes in more recent decades. Future research is needed to understand how the snow metric declines reported in this study relate to changes in runoff generation (e.g., Penn et al. 2020; Rumsey et al. 2020).

c. Snow metric sensitivities

The results from this study can be used to identify localized areas that exhibited the greatest snow metric sensitivity to change. We calculated snow metric sensitivity for each combination of elevation zone (100-m increments) and land-cover type (e.g., Fig. 6) based on the percentage change decade^{-1} scaled by the percentage of that zone with trends (Fig. 11). We used these results to identify the area (elevation and land-cover type) of peak sensitivity for each snow metric within the study
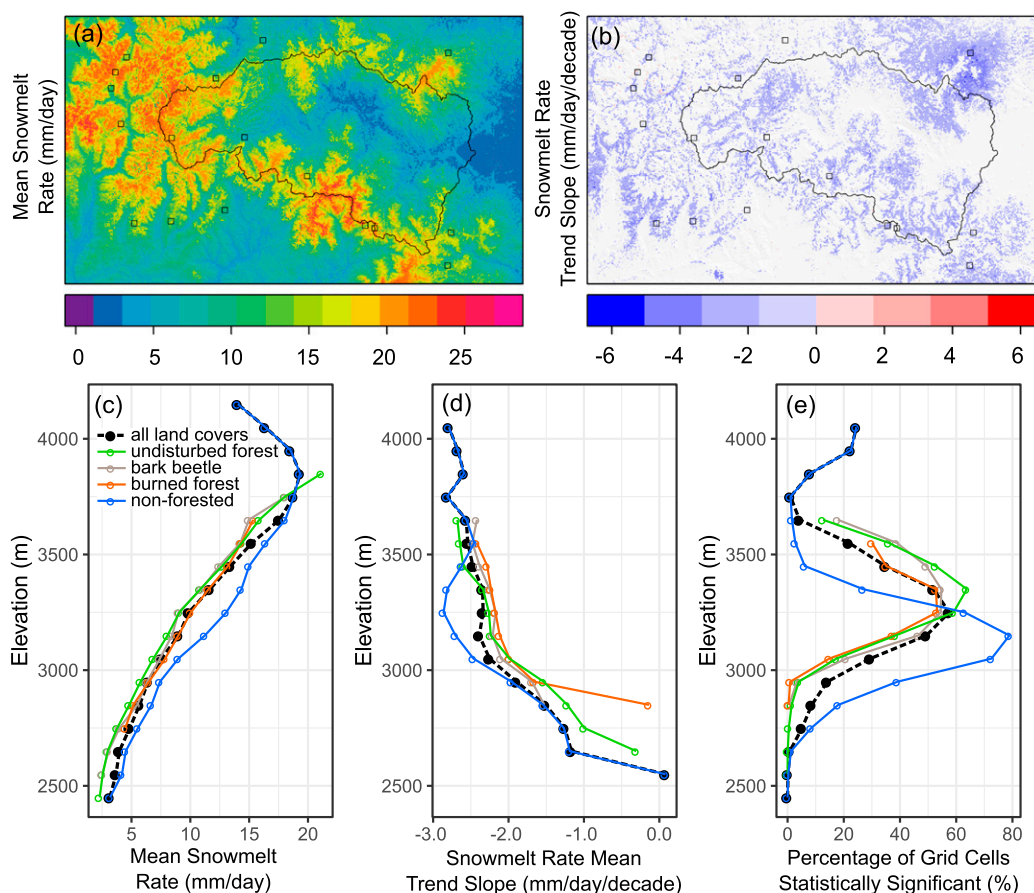
FIG. 8. As in Fig. 5, but for simulated snowmelt rate (mm day^{-1}).

area (Fig. 11). Middle elevation forested areas showed the greatest sensitivity to changes in peak SWE and SWE:P. This is consistent with previous research indicating that midelevation snowpacks are most sensitive to climate warming (Nolin and Daly 2006; Sproles et al. 2013). These results have important implications for future water resource management because this is an area that holds substantial volumetric snow water storage (Fig. 6) and is also coincident with the location of most snow monitoring stations in the region (Molotch and Bales 2006). Low and middle elevation forests that were burned by the 2013 wildfire in the basin showed the greatest sensitivity to sublimation losses and snowmelt timing metrics (Fig. 11). Widespread downward trends in sublimation at these elevations as a result of reductions in snow-cover duration were further magnified by the loss of canopy-intercepted snow and subsequent canopy sublimation in burned forests. Similarly, downward trends in snowmelt timing were magnified in burned forests as a result of the postfire radiative forcing simulated in this study that enhanced albedo decay and advanced snowmelt timing (Gleason and Nolin 2016; Gleason et al. 2013). Total snowmelt amount as well as the effective sublimation was found to be most sensitive in the high-elevation alpine areas. High-elevation areas have generally been indicated to be the most resilient areas to changing

snowpack conditions (IPCC 2019). However, the combined effect of upward winter T trends, downward winter P trends, and the increased effective sublimation at the highest elevations in this study indicates that decreased springtime snow accumulation following peak SWE as well as changing sublimation processes may play an important role in the sensitivity of snowmelt to changes in climate.

d. Uncertainties

The simulated snow trends reported in this study were largely driven by the NLDAS-2 atmospheric forcing data that were used. As a result, any uncertainties associated with the assimilated observational datasets, temporal data discontinuities, and/or model physics in the NLDAS-2 forcing data were likely to propagate to the SnowModel simulations (Liston and Hiemstra 2011; Raleigh et al. 2015, 2016). However, NLDAS-2 is rigorously evaluated and developed to provide spatially and temporally consistent datasets from available observations and reanalyses to support modeling activities (Mitchell et al. 2004; Xia et al. 2012), and has been used recently by other studies conducting trend analyses (Girotto et al. 2017; Jasinski et al. 2019; Khaki and Awange 2019; Khaki et al. 2018). The simulated winter T trends presented in this study on the order of 0.3°C decade^{-1} are comparable to the homogenized T trends
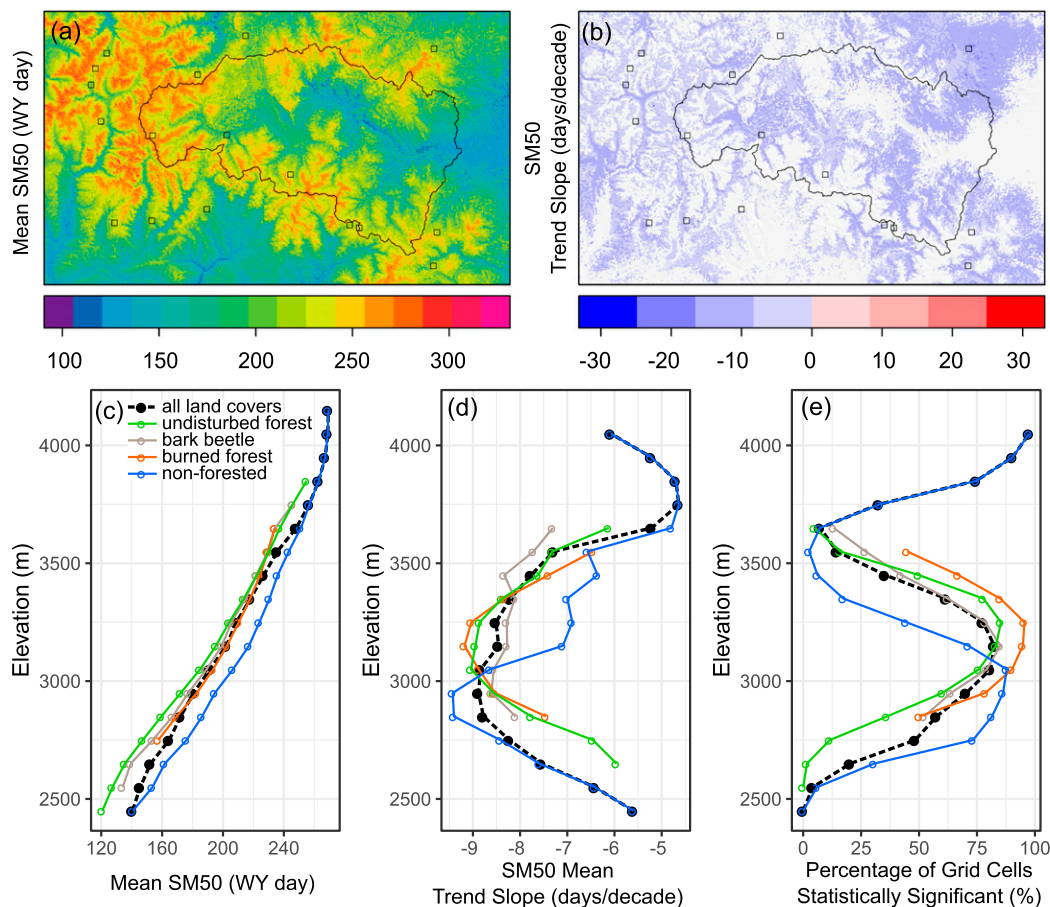
FIG. 9. As in Fig. 5, but for simulated SM50 (WY day).

presented by Oyler et al. (2015) and Ma et al. (2019) for this region and indicate that the NLDAS-2 *T* dataset was not subjected to artificial warming trends that were the result of a *T* sensor change at SNOTEL stations (Ma et al. 2019; Oyler et al. 2015). Biases in NLDAS-2 *P* have been reported by previous studies for this region (Henn et al. 2018; Sexstone et al. 2018). Given the importance of winter *P* forcing to SnowModel simulation accuracy, we used the SnowAssim (Liston and Hiemstra 2008) data assimilation scheme to adjust the simulated winter *P* for each year of the model simulations based on SWE observations to minimize these model biases (Table S3). Our trend results provide strong comparisons to SNOTEL observations in the domain indicating limited *P* biases in this study (Table 2; Fig. 2). Station observations of atmospheric humidity also compared well to model simulations (Table 2). The moderate correlation and low bias between simulated and observed wind speeds additionally provides confidence in the model representation of surface winds (Table 2). However, improvements in simulated wind speed performance with increasing elevation (Fig. S2) indicates uncertainties in model downscaling of surface winds. Furthermore, potential scaling issues associated with 100-m resolution grid cells not being fine enough resolution to adequately resolve wind redistribution processes (Mott et al. 2018)

likely contributed to uncertainties in simulated snow distributions in alpine areas in this study (Fig. 4). Therefore, in the context of our trend results highlighting an increasing importance of relative sublimation fluxes to snowmelt sensitivity in these areas, further research is needed to help constrain the uncertainties in wind redistribution and sublimation processes in alpine areas to further evaluate alpine snow sensitivities to changing climate.

The vegetation change parameterization used is this study likely oversimplified the actual changes in surface conditions within the study area. In addition to the difficulty of accurately representing the spatial variability of vegetation disturbance severity and response using the linear scaling of LAI*, this study also did not consider changes in land cover through time associated with land management practices and logging. Furthermore, this work smooths some forest snow processes that happen at scales finer than 100 m (e.g., Broxton et al. 2015). Interacting forest structure metrics such as canopy gaps and edges can result in high spatial snow heterogeneity due to a complex interplay between accumulation and ablation processes (e.g., Pomeroy et al. 2009; Veatch et al. 2009; Moeser et al. 2016). Further research is needed to develop subgrid model representations from widely available datasets of these finescale canopy snow processes (e.g., Mazzotti et al. 2020).
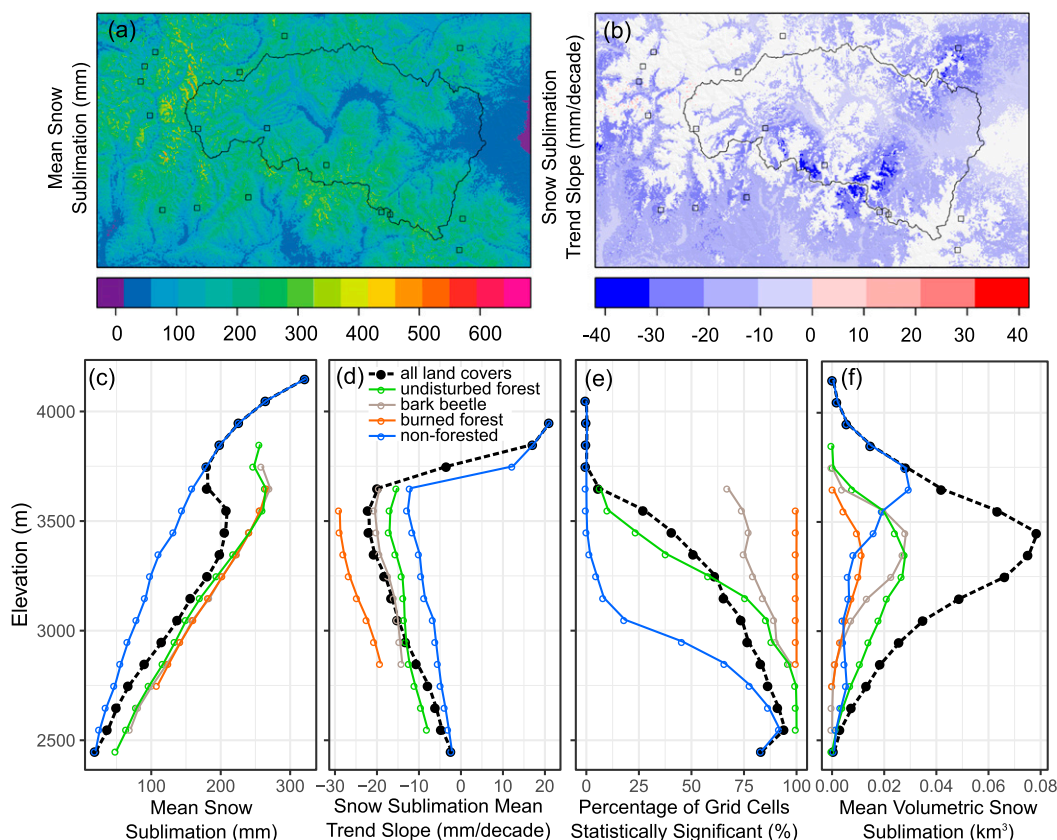
FIG. 10. As in Fig. 6, but for simulated snow sublimation.

Despite the uncertainties related to the representation of vegetation across the study area, the SnowModel simulations presented here displayed a good fit to ground-based observations across a range of different land-cover types that support the estimates of changing snow dynamics across the basin extent presented herein.

5. Conclusions

SnowModel simulations were run over a 34-yr period (1984–2017) at 100-m spatial resolution to evaluate the spatial variability of trends in simulated snowpack properties across the Rio Grande headwaters. Model evaluations based on snow and meteorological station observations, field-based snow observations, and spatially distributed remote sensing observations of SCA and SWE were used to show that the SnowModel simulations reasonably represented observed snow-station trends within the model domain as well as the spatial distribution of snowpack properties across the study basin. Trends in simulated snow metrics computed in this study exhibited widespread declines, but also exhibited spatial variability related to elevation, aspect, and land cover. Trends were not found to occur everywhere within the basin, and some areas were more sensitive than others with distinct differences between snow metrics. Upward trends in mean winter T of approximately 0.3°C decade^{-1} were consistent

across the study area, whereas downward trends in winter P ranged from −35 to −76 mm decade^{-1} with the greatest magnitude decreases occurring at the highest elevations. Elevation-dependent trends in T and P resulted in an elevation dependence in snow metric trends with middle elevations (coincident with the greatest volumetric snow water storage) exhibiting the greatest sensitivity to changes in peak SWE in forested areas, snowmelt rate in nonforested areas, and metrics associated with snowmelt timing in burned forest areas. At the lowest elevations, decreases in snow-covered days in nonforested areas and sublimation losses in burned forest areas were most sensitive to change. Within high-elevation alpine areas, decreases in total snowmelt quantity and increases in effective sublimation were most sensitive to change, indicating an increasing importance of decreasing late-season snow accumulation and relative sublimation fluxes in these areas. Across the Rio Grande headwaters, snowmelt rates decreased by 20% decade^{-1}, peak SWE decreased by 14% decade^{-1}, and total snowmelt amount decreased by 13% decade^{-1}. Snow trends presented in this study are in general agreement with widespread snow declines that have been reported for this region and provide further evidence for these recent trends across a greater spatial coverage with finer spatial resolution. Given the importance of adequate accounting of snow storage across the basin scale, results from this study have important
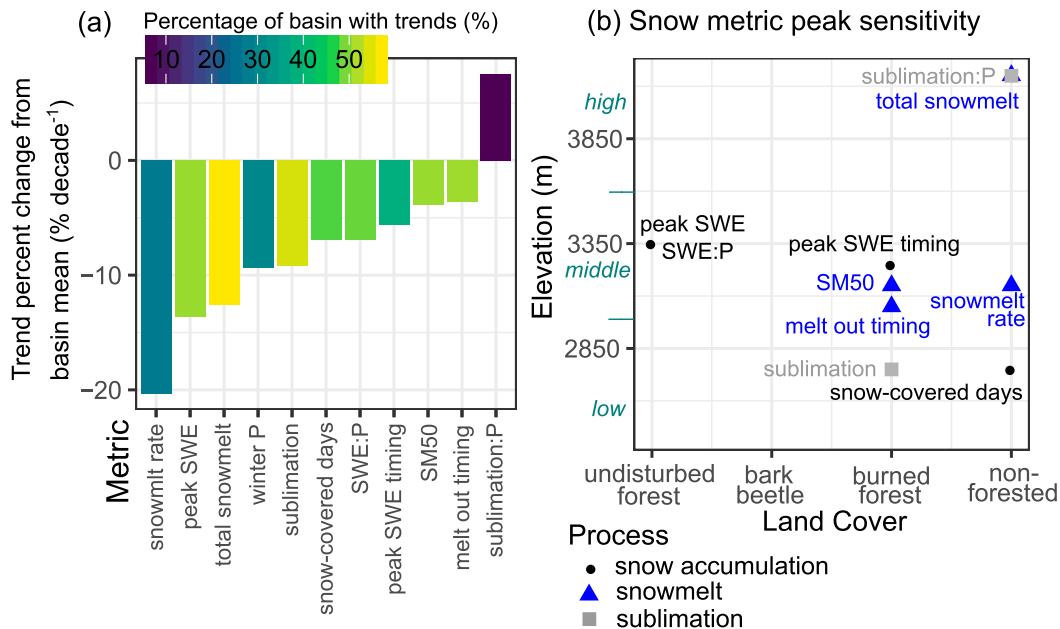
FIG. 11. (a) Percentage change per decade for each snow metric (normalized mean snow metric trends by the basin mean for areas with trends over the period of analysis) colored by the percentage of the study area with statistically significant trends. (b) The elevation and land cover combination yielding the peak sensitivity (percentage change per decade normalized by the percentage of area with statistically significant trends) for each snow metric. [e.g., peak SWE is plotted in (b) for forested areas at elevations between 3300 and 3400 m (North American Vertical Datum of 1988) as this was the region with the greatest sensitivity for that snow metric].

implications for future investigations into snow–hydrology–climate interactions and are relevant to future water management planning.

REFERENCES

Auer, A. H., 1974: The rain versus snow threshold temperatures. *Weatherwise*, **27**, 67, https://doi.org/10.1080/00431672.1974.9931684.
Barnett, T. P., J. C. Adam, and D. P. Lettenmaier, 2005: Potential impacts of a warming climate on water availability in snow-dominated regions. *Nature*, **438**, 303–309, https://doi.org/10.1038/nature04141.
Biederman, J. A., P. D. Brooks, A. A. Harpold, D. J. Gochis, E. Gutmann, D. E. Reed, E. Pendall, B. E. Ewers, 2014: Multiscale observations of snow accumulation and peak snowpack following widespread, insect-induced lodgepole pine mortality. *Ecohydrology*, **7**, 150–162, https://doi.org/10.1002/eco.1342.
Blöschl, G., 1999: Scaling issues in snow hydrology. *Hydrol. Processes*, **13**, 2149–2175, https://doi.org/10.1002/(SICI)1099-1085(199910)13:14/15<2149::AID-HYP847>3.0.CO;2-8.
Bright, B. C., J. A. Hicke, and A. J. H. Meddens, 2013: Effects of bark beetle-caused tree mortality on biogeochemical and biogeophysical MODIS products. *J. Geophys. Res. Biogeosci.*, **118**, 974–982, https://doi.org/10.1002/jgrg.20078.
Broxton, P. D., A. A. Harpold, J. A. Biederman, P. A. Troch, N. P. Molotch, and P. D. Brooks, 2015: Quantifying the effects of vegetation structure on snow accumulation and ablation in mixed-conifer forests. *Ecohydrology*, **8**, 1073–1094, https://doi.org/10.1002/eco.1565.
Chavarria, S. B., and D. S. Gutzler, 2018: Observed changes in climate and streamflow in the Upper Rio Grande Basin. *J. Amer. Water Resour. Assoc.*, **54**, 644–659, https://doi.org/10.1111/1752-1688.12640.
Clow, D. W., 2010: Changes in the timing of snowmelt and streamflow in Colorado: A response to recent warming. *J. Climate*, **23**, 2293–2306, https://doi.org/10.1175/2009JCLI2951.1.
Deems, J. S., S. R. Fassnacht, and K. J. Elder, 2006: Fractal distribution of snow depth from lidar data. *J. Hydrometeor.*, **7**, 285–297, https://doi.org/10.1175/JHM487.1.
Eidenshink, J., B. Schwind, K. Brewer, Z.-L. Zhu, B. Quayle, and S. Howard, 2007: A project for monitoring trends in burn severity. *Fire Ecol.*, **3**, 3–21, https://doi.org/10.4996/fireecology.0301003.

Elder, K., J. Dozier, and J. Michaelsen, 1991: Snow accumulation and distribution in an alpine watershed. *Water Resour. Res.*, **27**, 1541–1552, https://doi.org/10.1029/91WR00506.

Ellis, C. R., J. W. Pomeroy, and T. E. Link, 2013: Modeling increases in snowmelt yield and desynchronization resulting from forest gap-thinning treatments in a northern mountain headwater basin. *Water Resour. Res.*, **49**, 936–949, https://doi.org/10.1002/wrcr.20089.

Fassnacht, S., N. Venable, D. McGrath, and G. Patterson, 2018: Sub-seasonal snowpack trends in the Rocky Mountain National Park area, Colorado, USA. *Water*, **10**, 562, https://doi.org/10.3390/w10050562.

Fletcher, S. J., G. E. Liston, C. A. Hiemstra, and S. D. Miller, 2012: Assimilating MODIS and AMSR-E snow observations in a snow evolution model. *J. Hydrometeor.*, **13**, 1475–1492, https://doi.org/10.1175/JHM-D-11-082.1.

Frank, J. M., W. J. Massman, B. E. Ewers, and D. G. Williams, 2019: Bayesian analyses of 17 winters of water vapor fluxes show bark beetles reduce sublimation. *Water Resour. Res.*, **55**, 1598–1623, https://doi.org/10.1029/2018WR023054.

Fritze, H., I. T. Stewart, and E. Pebesma, 2011: Shifts in western North American snowmelt runoff regimes for the recent warm decades. *J. Hydrometeor.*, **12**, 989–1006, https://doi.org/10.1175/2011JHM1360.1.

Furniss, M. J., and Coauthors, 2010: Water, climate change, and forests: Watershed stewardship for a changing climate. General Tech. Rep. PNW-GTR-812, 75 pp., https://www.fs.fed.us/pnw/pubs/pnw_gtr812.pdf.

Gascoin, S., S. Lhermitte, C. Kinnard, K. Bortels, and G. E. Liston, 2013: Wind effects on snow cover in Pascua-Lama, Dry Andes of Chile. *Adv. Water Resour.*, **55**, 25–39, https://doi.org/10.1016/j.advwatres.2012.11.013.

Girotto, M., G. J. M. De Lannoy, R. H. Reichle, M. Rodell, C. Draper, S. N. Bhanja, and A. Mukherjee, 2017: Benefits and pitfalls of GRACE data assimilation: A case study of terrestrial water storage depletion in India. *Geophys. Res. Lett.*, **44**, 4107–4115, https://doi.org/10.1002/2017GL072994.

Gleason, K. E., and A. W. Nolin, 2016: Charred forests accelerate snow albedo decay: Parameterizing the post-fire radiative forcing on snow for three years following fire. *Hydrol. Processes*, **30**, 3855–3870, https://doi.org/10.1002/hyp.10897.

——, ——, and T. R. Roth, 2013: Charred forests increase snowmelt: Effects of burned woody debris and incoming solar radiation on snow ablation. *Geophys. Res. Lett.*, **40**, 4654–4661, https://doi.org/10.1002/grl.50896.

——, ——, and ——, 2017: Developing a representative snow-monitoring network in a forested mountain watershed. *Hydrol. Earth Syst. Sci.*, **21**, 1137–1147, https://doi.org/10.5194/hess-21-1137-2017.

——, J. R. McConnell, M. M. Arienzo, N. Chellman, and W. M. Calvin, 2019: Four-fold increase in solar forcing on snow in western US burned forests since 1999. *Nat. Commun.*, **10**, 2026, https://doi.org/10.1038/s41467-019-09935-y.

Greene, E. M., G. E. Liston, and R. A. Pielke, 1999: Simulation of above treeline snowdrift formation using a numerical snow-transport model. *Cold Reg. Sci. Technol.*, **30**, 135–144, https://doi.org/10.1016/S0165-232X(99)00008-7.

Hammond, J. C., F. A. Saavedra, and S. K. Kampf, 2018a: How does snow persistence relate to annual streamflow in mountain watersheds of the western U.S. with wet maritime and dry continental climates? *Water Resour. Res.*, **54**, 2605–2623, https://doi.org/10.1002/2017WR021899.

——, ——, and ——, 2018b: Global snow zone maps and trends in snow persistence 2001-2016. *Int. J. Climatol.*, **38**, 4369–4383, https://doi.org/10.1002/joc.5674.

Harpold, A. A., and P. D. Brooks, 2018: Humidity determines snowpack ablation under a warming climate. *Proc. Natl. Acad. Sci. USA*, **115**, 1215–1220, https://doi.org/10.1073/pnas.1716789115.

——, P. Brooks, S. Rajagopal, I. Heidbuchel, A. Jardine, and C. Stielstra, 2012: Changes in snowpack accumulation and ablation in the Intermountain West. *Water Resour. Res.*, **48**, W11501, https://doi.org/10.1029/2012WR011949.

——, and Coauthors, 2014: Changes in snow accumulation and ablation following the Las Conchas Forest Fire, New Mexico, USA. *Ecohydrology*, **7**, 440–452, https://doi.org/10.1002/eco.1363.

Hedrick, A. R., and Coauthors, 2018: Direct insertion of NASA Airborne Snow Observatory-derived snow depth time series into the iSnobal energy balance snow model. *Water Resour. Res.*, **54**, 8045–8063, https://doi.org/10.1029/2018WR023190.

Henn, B., A. J. Newman, B. Livneh, C. Daly, and J. D. Lundquist, 2018: An assessment of differences in gridded precipitation datasets in complex terrain. *J. Hydrol.*, **556**, 1205–1219, https://doi.org/10.1016/j.jhydrol.2017.03.008.

Hiemstra, C. A., G. E. Liston, and W. A. Reiners, 2006: Observing, modelling, and validating snow redistribution by wind in a Wyoming upper treeline landscape. *Ecol. Modell.*, **197**, 35–51, https://doi.org/10.1016/j.ecolmodel.2006.03.005.

Homer, C., and Coauthors, 2015: Completion of the 2011 National Land Cover Database for the conterminous United States - Representing a decade of land cover change information. *Photogramm. Eng. Remote Sens.*, **81**, 345–354.

IPCC, 2019: IPCC special report on the ocean and cryosphere in a changing climate. H.-O. Pörtner et al., Eds., IPCC, 755 pp., https://www.ipcc.ch/srocc/.

Jasinski, M. F., and Coauthors, 2019: NCA-LDAS: Overview and analysis of hydrologic trends for the National Climate Assessment. *J. Hydrometeor.*, **20**, 1595–1617, https://doi.org/10.1175/JHM-D-17-0234.1.

Khaki, M., and J. Awange, 2019: The application of multi-mission satellite data assimilation for studying water storage changes over South America. *Sci. Total Environ.*, **647**, 1557–1572, https://doi.org/10.1016/j.scitotenv.2018.08.079.

——, E. Forootan, M. Kuhn, J. Awange, A. I. J. M. van Dijk, M. Schumacher, and M. A. Sharifi, 2018: Determining water storage depletion within Iran by assimilating GRACE data into the W3RA hydrological model. *Adv. Water Resour.*, **114**, 1–18, https://doi.org/10.1016/j.advwatres.2018.02.008.

Kinar, N. J., and J. W. Pomeroy, 2015: Measurement of the physical properties of the snowpack. *Rev. Geophys.*, **53**, 481–544, https://doi.org/10.1002/2015RG000481.

Knowles, J. F., and Coauthors, 2015: The relative contributions of alpine and subalpine ecosystems to the water balance of a mountainous, headwater catchment. *Hydrol. Processes*, **29**, 4794–4808, https://doi.org/10.1002/hyp.10526.

Knowles, N., M. D. Dettinger, and D. R. Cayan, 2006: Trends in snowfall versus rainfall in the western United States. *J. Climate*, **19**, 4545–4559, https://doi.org/10.1175/JCLI3850.1.

Kunkel, K. E., D. A. Robinson, S. Champion, X. G. Yin, T. Estilow, and R. M. Frankson, 2016: Trends and extremes in northern hemisphere snow characteristics. *Curr. Climate Change Rep.*, **2**, 65–73, https://doi.org/10.1007/s40641-016-0036-8.

Lehner, F., E. R. Wahl, A. W. Wood, D. B. Blatchford, and D. Llewellyn, 2017: Assessing recent declines in Upper Rio Grande runoff efficiency from a paleoclimate perspective.

Geophys. Res. Lett., **44**, 4124–4133, https://doi.org/10.1002/2017GL073253.

Li, D., M. L. Wrzesien, M. Durand, J. Adam, and D. P. Lettenmaier, 2017: How much runoff originates as snow in the western United States, and how will that change in the future? *Geophys. Res. Lett.*, **44**, 6163–6172, https://doi.org/10.1002/2017GL073551.

Liston, G. E., 1995: Local advection of momentum, heat, and moisture during the melt of patchy snow covers. *J. Appl. Meteor.*, **34**, 1705–1715, https://doi.org/10.1175/1520-0450-34.7.1705.

——, and D. K. Hall, 1995: An energy-balance model of lake-ice evolution. *J. Glaciol.*, **41**, 373–382, https://doi.org/10.1017/S0022143000016245.

——, and M. Sturm, 1998: A snow-transport model for complex terrain. *J. Glaciol.*, **44**, 498–516, https://doi.org/10.1017/S0022143000002021.

——, and K. Elder, 2006a: A meteorological distribution system for high-resolution terrestrial modeling (MicroMet). *J. Hydrometeor.*, **7**, 217–234, https://doi.org/10.1175/JHM486.1.

——, and ——, 2006b: A distributed snow-evolution modeling system (SnowModel). *J. Hydrometeor.*, **7**, 1259–1276, https://doi.org/10.1175/JHM548.1.

——, and C. A. Hiemstra, 2008: A simple data assimilation system for complex snow distributions (SnowAssim). *J. Hydrometeor.*, **9**, 989–1004, https://doi.org/10.1175/2008JHM871.1.

——, and ——, 2011: The changing cryosphere: Pan-Arctic snow trends (1979–2009). *J. Climate*, **24**, 5691–5712, https://doi.org/10.1175/JCLI-D-11-00081.1.

——, R. B. Haehnel, M. Sturm, C. A. Hiemstra, S. Berezovskaya, and R. D. Tabler, 2007: Simulating complex snow distributions in windy environments using SnowTran-3D. *J. Glaciol.*, **53**, 241–256, https://doi.org/10.3189/172756507782202865.

——, C. A. Hiemstra, K. Elder, and D. W. Cline, 2008: Mesocell study area snow distributions for the Cold Land Processes Experiment (CLPX). *J. Hydrometeor.*, **9**, 957–976, https://doi.org/10.1175/2008JHM869.1.

——, C. Polashenski, A. Rosel, P. Itkin, J. King, I. Merkouriadi, and J. Haapala, 2018: A distributed snow-evolution model for sea-ice applications (SnowModel). *J. Geophys. Res. Oceans*, **123**, 3786–3810, https://doi.org/10.1002/2017JC013706.

López-Moreno, J. I., S. R. Fassnacht, S. Beguería, and J. B. P. Latron, 2011: Variability of snow depth at the plot scale: Implications for mean depth estimation and sampling strategies. *Cryosphere*, **5**, 617–629, https://doi.org/10.5194/tc-5-617-2011.

——, J. Revuelto, S. R. Fassnacht, C. Azorin-Molina, S. M. Vicente-Serrano, E. Moran-Tejeda, and G. A. Sexstone, 2015: Snowpack variability across various spatio-temporal resolutions. *Hydrol. Processes*, **29**, 1213–1224, https://doi.org/10.1002/hyp.10245.

——, and Coauthors, 2017: Different sensitivities of snowpacks to warming in Mediterranean climate mountain areas. *Environ. Res. Lett.*, **12**, 074006, https://doi.org/10.1088/1748-9326/aa70cb.

——, and Coauthors, 2020: Long-term trends (1958–2017) in snow cover duration and depth in the Pyrenees. *Int. J. Climatol.*, https://doi.org/10.1002/joc.6571, in press.

Ma, C., S. R. Fassnacht, and S. K. Kampf, 2019: How temperature sensor change affects warming trends and modeling: An evaluation across the state of Colorado. *Water Resour. Res.*, **55**, 9748–9764, https://doi.org/10.1029/2019WR025921.

MacDonald, M. K., J. W. Pomeroy, and A. Pietroniro, 2010: On the importance of sublimation to an alpine snow mass balance in the Canadian Rocky Mountains. *Hydrol. Earth Syst. Sci.*, **14**, 1401–1415, https://doi.org/10.5194/hess-14-1401-2010.

Mann, H. B., 1945: Non-parametric tests against trend. *Econometrica*, **13**, 245–259, https://doi.org/10.2307/1907187.

Marchetto, A., 2017: rkt: Mann-Kendall test, seasonal and regional Kendall tests, version 1.5. R package, https://CRAN.R-project.org/package=rkt.

Margulis, S. A., G. Cortes, M. Girotto, and M. Durand, 2016: A Landsat-era Sierra Nevada snow reanalysis (1985–2015). *J. Hydrometeor.*, **17**, 1203–1221, https://doi.org/10.1175/JHM-D-15-0177.1.

Mazzotti, G., R. Essery, C. D. Moeser, and T. Jonas, 2020: Resolving small-scale forest snow patterns using an energy balance snow model with a one-layer canopy. *Water Resour. Res.*, **56**, e2019WR026129, https://doi.org/10.1029/2019WR026129.

McCabe, G. J., and M. P. Clark, 2005: Trends and variability in snowmelt runoff in the western United States. *J. Hydrometeor.*, **6**, 476–482, https://doi.org/10.1175/JHM428.1.

Meromy, L., N. P. Molotch, T. E. Link, S. R. Fassnacht, and R. Rice, 2013: Subgrid variability of snow water equivalent at operational snow stations in the western USA. *Hydrol. Processes*, **27**, 2383–2400, https://doi.org/10.1002/hyp.9355.

Middelkoop, H., and Coauthors, 2001: Impact of climate change on hydrological regimes and water resources management in the Rhine basin. *Climatic Change*, **49**, 105–128, https://doi.org/10.1023/A:1010784727448.

Mitchell, K. E., and Coauthors, 2004: The multi-institution North American Land Data Assimilation System (NLDAS): Utilizing multiple GCIP products and partners in a continental distributed hydrological modeling system. *J. Geophys. Res.*, **109**, D07S90, https://doi.org/10.1029/2003JD003823.

Moeser, D., G. Mazzotti, N. Helbig, and T. Jonas, 2016: Representing spatial variability of forest snow: Implementation of a new interception model. *Water Resour. Res.*, **52**, 1208–1226, https://doi.org/10.1002/2015WR017961.

Molotch, N. P., 2009: Reconstructing snow water equivalent in the Rio Grande headwaters using remotely sensed snow cover data and a spatially distributed snowmelt model. *Hydrol. Processes*, **23**, 1076–1089, https://doi.org/10.1002/hyp.7206.

——, and R. C. Bales, 2005: Scaling snow observations from the point to the grid element: Implications for observation network design. *Water Resour. Res.*, **41**, W11421, https://doi.org/10.1029/2005WR004229.

——, and ——, 2006: SNOTEL representativeness in the Rio Grande headwaters on the basis of physiographics and remotely sensed snow cover persistence. *Hydrol. Processes*, **20**, 723–739, https://doi.org/10.1002/hyp.6128.

Morán-Tejeda, E., J. I. López-Moreno, and M. Beniston, 2013: The changing roles of temperature and precipitation on snowpack variability in Switzerland as a function of altitude. *Geophys. Res. Lett.*, **40**, 2131–2136, https://doi.org/10.1002/grl.50463.

Mote, P. W., 2006: Climate-driven variability and trends in mountain snowpack in western North America. *J. Climate*, **19**, 6209–6220, https://doi.org/10.1175/JCLI3971.1.

——, A. F. Hamlet, M. P. Clark, and D. P. Lettenmaier, 2005: Declining mountain snowpack in western North America. *Bull. Amer. Meteor. Soc.*, **86**, 39–50, https://doi.org/10.1175/BAMS-86-1-39.

——, S. Li, D. P. Lettenmaier, M. Xiao, and R. Engel, 2018: Dramatic declines in snowpack in the western US. *npj Climate Atmos. Sci.*, **1**, 2, https://doi.org/10.1038/s41612-018-0012-1.

Mott, R., V. Vionnet, and T. Grunewald, 2018: The seasonal snow cover dynamics: Review on wind-driven coupling

processes. *Front. Earth Sci.*, **6**, 197, https://doi.org/10.3389/feart.2018.00197.

Musselman, K. N., N. P. Molotch, and S. A. Margulis, 2017a: Snowmelt response to simulated warming across a large elevation gradient, southern Sierra Nevada, California. *Cryosphere*, **11**, 2847–2866, https://doi.org/10.5194/tc-11-2847-2017.

——, M. P. Clark, C. H. Liu, K. Ikeda, and R. Rasmussen, 2017b: Slower snowmelt in a warmer world. *Nat. Climate Change*, **7**, 214–219, https://doi.org/10.1038/nclimate3225.

Nolin, A. W., and C. Daly, 2006: Mapping "at risk" snow in the Pacific Northwest. *J. Hydrometeor.*, **7**, 1164–1171, https://doi.org/10.1175/JHM543.1.

Oyler, J. W., S. Z. Dobrowski, A. P. Ballantyne, A. E. Klene, and S. W. Running, 2015: Artificial amplification of warming trends across the mountains of the western United States. *Geophys. Res. Lett.*, **42**, 153–161, https://doi.org/10.1002/2014GL062803.

Painter, T. H., 2018: ASO L4 lidar snow water equivalent 50m UTM grid, version 1. NASA National Snow and Ice Data Center Distributed Active Archive Center, accessed 18 September 2019, https://doi.org/10.5067/M4TUH28NHL4Z.

——, S. M. Skiles, J. S. Deems, A. C. Bryant, and C. C. Landry, 2012: Dust radiative forcing in snow of the Upper Colorado River Basin: 1. A 6 year record of energy balance, radiation, and dust concentrations. *Water Resour. Res.*, **48**, W07521, https://doi.org/10.1029/2012WR011985.

——, and Coauthors, 2016: The Airborne Snow Observatory: Fusion of scanning lidar, imaging spectrometer, and physically-based modeling for mapping snow water equivalent and snow albedo. *Remote Sens. Environ.*, **184**, 139–152, https://doi.org/10.1016/j.rse.2016.06.018.

Penn, C. A., D. W. Clow, G. A. Sexstone, and S. F. Murphy, 2020: Changes in climate and land cover affect seasonal streamflow forecasts in the Rio Grande Headwaters. *J. Amer. Water Resour. Assoc.*, **56**, 882–902, https://doi.org/10.1111/1752-1688.12863.

Pomeroy, J. W., D. Marks, T. Link, C. Ellis, J. Hardy, A. Rowlands, and R. Granger, 2009: The impact of coniferous forest temperature on incoming longwave radiation to melting snow. *Hydrol. Processes*, **23**, 2513–2525, https://doi.org/10.1002/hyp.7325.

Potter, K. M., and B. L. Conkling, 2016: Forest health monitoring: National status, trends, and analysis 2015. General Tech. Rep. SRS-213, 199 pp., https://www.srs.fs.usda.gov/pubs/52181.

Prasad, R., D. G. Tarboton, G. E. Liston, C. H. Luce, and M. S. Seyfried, 2001: Testing a blowing snow model against distributed snow measurements at Upper Sheep Creek, Idaho, United States of America. *Water Resour. Res.*, **37**, 1341–1356, https://doi.org/10.1029/2000WR900317.

Pugh, E., and E. Small, 2012: The impact of pine beetle infestation on snow accumulation and melt in the headwaters of the Colorado River. *Ecohydrology*, **5**, 467–477, https://doi.org/10.1002/eco.239.

——, and E. Gordon, 2013: A conceptual model of water yield effects from beetle-induced tree death in snow-dominated lodgepole pine forests. *Hydrol. Processes*, **27**, 2048–2060, https://doi.org/10.1002/hyp.9312.

R Core Team, 2019: R: A language and environment for statistical computing. R Foundation for Statistical Computing, Vienna, Austria, https://www.R-project.org/.

Raleigh, M. S., J. D. Lundquist, and M. P. Clark, 2015: Exploring the impact of forcing error characteristics on physically based snow simulations within a global sensitivity analysis

framework. *Hydrol. Earth Syst. Sci.*, **19**, 3153–3179, https://doi.org/10.5194/hess-19-3153-2015.

——, B. Livneh, K. Lapo, and J. D. Lundquist, 2016: How does availability of meteorological forcing data impact physically based snowpack simulations? *J. Hydrometeor.*, **17**, 99–120, https://doi.org/10.1175/JHM-D-14-0235.1.

Rango, A., 2006: Snow: The real water supply for the Rio Grande Basin. *New Mexico J. Sci.*, **44**, 99–118.

Reba, M. L., J. Pomeroy, D. Marks, and T. E. Link, 2012: Estimating surface sublimation losses from snowpacks in a mountain catchment using eddy covariance and turbulent transfer calculations. *Hydrol. Processes*, **26**, 3699–3711, https://doi.org/10.1002/hyp.8372.

Regonda, S. K., B. Rajagopalan, M. Clark, and J. Pitlick, 2005: Seasonal cycle shifts in hydroclimatology over the western United States. *J. Climate*, **18**, 372–384, https://doi.org/10.1175/JCLI-3272.1.

Rumsey, C. A., M. P. Miller, and G. A. Sexstone, 2020: Relating hydroclimatic change to streamflow, baseflow, and hydrologic partitioning in the Upper Rio Grande Basin, 1980 to 2015. *J. Hydrol.*, **584**, 124715, https://doi.org/10.1016/j.jhydrol.2020.124715.

Sen, P. K., 1968: Estimates of the regression coefficient based on Kendall's tau. *J. Amer. Stat. Assoc.*, **63**, 1379–1389, https://doi.org/10.1080/01621459.1968.10480934.

Serreze, M. C., M. P. Clark, R. L. Armstrong, D. A. McGinnis, and R. S. Pulwarty, 1999: Characteristics of the western United States snowpack from Snowpack Telemetry (SNOTEL) data. *Water Resour. Res.*, **35**, 2145–2160, https://doi.org/10.1029/1999WR900090.

Sexstone, G. A., 2020: SnowModel simulations and supporting observations for the Rio Grande Headwaters (1984 - 2017). U.S. Geological Survey, https://doi.org/10.5066/P9Q8PYX1.

——, and S. R. Fassnacht, 2014: What drives basin scale spatial variability of snowpack properties in northern Colorado? *Cryosphere*, **8**, 329–344, https://doi.org/10.5194/tc-8-329-2014.

——, D. W. Clow, D. I. Stannard, and S. R. Fassnacht, 2016: Comparison of methods for quantifying surface sublimation over seasonally snow-covered terrain. *Hydrol. Processes*, **30**, 3373–3389, https://doi.org/10.1002/hyp.10864.

——, ——, S. R. Fassnacht, G. E. Liston, C. A. Hiemstra, J. F. Knowles, and C. A. Penn, 2018: Snow sublimation in mountain environments and its sensitivity to forest disturbance and climate warming. *Water Resour. Res.*, **54**, 1191–1211, https://doi.org/10.1002/2017WR021172.

Skiles, S. M., M. Flanner, J. M. Cook, M. Dumont, and T. H. Painter, 2018: Radiative forcing by light-absorbing particles in snow. *Nat. Climate Change*, **8**, 964–971, https://doi.org/10.1038/s41558-018-0296-5.

Sproles, E. A., A. W. Nolin, K. Rittger, and T. H. Painter, 2013: Climate change impacts on maritime mountain snowpack in the Oregon Cascades. *Hydrol. Earth Syst. Sci.*, **17**, 2581–2597, https://doi.org/10.5194/hess-17-2581-2013.

Stewart, I. T., 2009: Changes in snowpack and snowmelt runoff for key mountain regions. *Hydrol. Processes*, **23**, 78–94, https://doi.org/10.1002/hyp.7128.

USFS, 2016: Insect and Disease Detection Survey. Forest Service, USDA, https://www.fs.fed.us/foresthealth/applied-sciences/mapping-reporting/detection-surveys.shtml.

Veatch, W., P. D. Brooks, J. R. Gustafson, and N. Molotch, 2009: Quantifying the effects of forest canopy cover on net snow accumulation at a continental, mid-latitude site. *Ecohydrology*, **2**, 115–128, https://doi.org/10.1002/eco.45.

Vionnet, V., E. Martin, V. Masson, C. Lac, F. N. Bouvet, and G. Guyomarc'h, 2017: High-resolution large eddy simulation

of snow accumulation in alpine terrain. *J. Geophys. Res. Atmos.*, **122**, 11 005–11 021, https://doi.org/10.1002/2017JD026947.

Westerling, A. L., H. G. Hidalgo, D. R. Cayan, and T. W. Swetnam, 2006: Warming and earlier spring increase western U.S. forest wildfire activity. *Science*, **313**, 940–943, https://doi.org/10.1126/science.1128834.

Xia, Y., and Coauthors, 2012: Continental-scale water and energy flux analysis and validation for the North American Land Data Assimilation System project phase 2 (NLDAS-2): 1. Intercomparison and application of model products.

J. Geophys. Res., **117**, D03109, https://doi.org/10.1029/2011JD016048.

Zambrano-Bigiarini, M., 2017: hydroGOF: Goodness-of-fit functions for comparison of simulated and observed hydrological time series, version 0.3-10. R package, http://hzambran.github.io/hydroGOF/.

Zeng, X. B., P. Broxton, and N. Dawson, 2018: Snowpack change from 1982 to 2016 over conterminous United States. *Geophys. Res. Lett.*, **45**, 12 940–12 947, https://doi.org/10.1029/2018GL079621.